Article

Structure–Properties Relationship of Reprocessed Bionanocomposites of Plasticized Polylactide Reinforced with Nanofibrillated Cellulose

O. Gil-Castell [1],*, M. H. Wolf [1], J. Cea [2], J. C. Carrasco [2], M. Giacinti Baschetti [3] and A. Ribes-Greus [1]

[1] Instituto de Tecnología de Materiales (ITM), Universitat Politècnica de València (UPV), Camino de Vera, s/n, 46022 Valencia, Spain

[2] Unidad de Desarrollo Tecnológico (UDT), Universidad de Concepción, Avenida Cordillera, 3624, Parque Industrial Coronel, Coronel 4191996, Chile

[3] Dipartimento di Ingegneria Civile, Chimica, Ambientale e dei Materiali (DICAM), Alma Mater Studiorum-Università di Bologna, Via Terracini, 28, 40131 Bologna, Italy

*   Correspondence: ogilcastell@doctor.upv.es

Abstract: Bionanocomposites of polylactide (PLA), plasticized with poly(ethylene glycol) (PEG) (7.5 wt%, 400 and 1500 g/mol) and reinforced with nanofibrillated cellulose (NFC) (1, 3, and 5 wt%) were sequentially compounded, and injection and compression molded. All of the stages caused structural and morphological consequences, more relevant in the plasticized PLA, especially with low molar PEG. Small percentages of NFC (1 and 3 wt%) acted as crystalline nucleating agents and improved thermo-oxidative stability. Given the substantial degradation caused by (re)processing, a downgrading validation strategy was applied, assessing the mechanical and water contact performance during fictional first and second service life applications. After the first processing, PEG increased the ductility and reduced the strength and elastic modulus, while NFC buffered the fall in stiffness and increased rigidity compared to their PLA-PEG counterparts. Once reprocessed, PEG increased the water affinity of the blend, especially for low molar mass PEG. Low percentages of NFC (1 and 3 wt%) modulated water diffusivity and permeability, regardless of the water temperature. Overall, although reprocessing caused significant degradation, the mechanical valorization possibilities of these green bionanocomposites were proven, and are pointed out as sustainable candidates for food packaging or agricultural applications where modulated mechanical or water contact behaviors are required.

Keywords: bionanocomposites; valorization; reprocessing; mechanical recycling; downgrading

1. Introduction

Biopolymers comprise a sustainable alternative and promising opportunity for almost every conventional fossil-based plastic application. Among the biopolymers, poly(lactide) (PLA) has been the frontrunner due to its attractive properties that meet the demands in packaging, agriculture, biomedicine, or automotive applications [1,2]. PLA can be made from agricultural products such as corn, sugar beets, and wheat, is easily biodegradable, and can be processed through conventional techniques due to its comparable rheological properties to traditional polymers. Although the use of PLA is growing, its actual contribution to the plastic industry is still limited due to shortcomings, especially related to its mechanical behavior or water permeability. The low deformation at break and high modulus restricted its application to the rigid thermoformed industry. Morphologies such as films or sheets usually require high flexibility at room temperature, transparency, and high barrier properties. Several strategies have been proposed to overcome these issues. The relatively stiff and brittle nature of PLA can be improved by modifying its physical properties through copolymerization with other monomers, blending with other polymers, and plasticization strategies [3,4].

Among the low molecular weight plasticizers for PLA [5–16], poly(ethylene glycol) (PEG) is one of the most suitable candidates due to its good miscibility with PLA, improvement of chain mobility, biodegradability, and allowed use in food-contactable applications [17–20]. The combination of PLA and small percentages of PEG up to 10% demonstrated complete miscibility, promoted a decrease in the tensile strength and elasticity modulus, and endorsed higher elongation at break and impact resistance. In this regard, the PEG molar mass has been identified as a relevant feature in the physico-chemical performance of plasticized PLA [8,21]. However, other characteristics, including thermal stability and water swelling, and diffusion in PLA/PEG blends, are still the target of optimization for widening the application of such alternatives.

Reinforcing PLA-based materials with natural fillers has been explored for the generation of green composites [22–24]. Cellulose-based reinforcements are among the most promising renewable fillers, especially concerning availability and biodegradability, which can modulate mechanical or permeability performance, among others [25–29]. Nanofibrillated cellulose (NFC) is an attractive renewable nanomaterial with a high surface-to-volume ratio, crystallinity, anisotropic performance, surface functionality, and excellent mechanical properties [30]. When hydrophobic matrices such as PLA are combined with hydrophilic fillers such as NFC, dispersion and compatibility concerns must be addressed through the surface functionalization of NFC or using coupling agents that allow for the proper interaction of both components in the composite. In this line, the acetylation of NFC and using PEG as a plasticizer and compatibilizer may become a sustainable alternative for spreading the use of PLA/NFC bionanocomposites.

The preparation and processing of bionanocomposites are critical stages because they define their properties and behaviors [22,31]. Several strategies have been reported for building products made of bionanocomposites, including filament winding, electrospinning, solution casting, 3D printing, extrusion, injection, or compression molding [32]. In particular, injection or compression molding are some of the most extended industrial processing setups. Both methods involve heat and pressure, which can cause mechanical and thermal degradation in PLA-based materials. The consequences of reprocessing PLA have been the center of numerous studies and highlighted thermo-mechanical degradation [33]. Mainly, changes in the structure and morphology caused by chain scission and inter/intramolecular transesterifications, inducing changes in its chemical, thermal, mechanical, and rheologic properties, have been reported [34,35]. As a whole, a significant performance loss after applying the second processing step was described, thus suggesting a drawback for the mechanical recycling of PLA. Several strategies have been explored to overcome these issues, including physical and chemical modifications, using stabilizers, chain extenders, reactive extrusion, and blending and compositing with other constituents [36–42]. For instance, Scaffaro et al. improved PLA's flexural and impact mechanical performance after multiple recycling steps using low percentages (8 wt%) of impact modifiers [43].

Particularly for PEG-plasticized PLA, research on reprocessing or recycling strategies is scarce, and only limited studies dealt with this topic, all of them considering reactive extrusion for the plasticization of PLA. Pascual-Jose et al. demonstrated that the addition of grafted acryl-poly(ethylene glycol) (acryl-PEG) during reactive extrusion was relevant to the molecular dynamics and segmental cooperativity of PLA, even more significant than the consequences of reprocessing, which contributed to reducing the dynamic fragility and increasing the PLA embrittlement after each reprocessing cycle [44]. In this regard, Brüster et al. also studied plasticized PLA with grafted acryl-PEG by reactive extrusion after several combined extrusion/compression molding cycles as a reprocessing strategy. They found that plasticized PLA underlay a more potent chain scission phenomenon (nearly double) than the neat PLA and concluded that at the current state, plasticized PLA by reactive extrusion could not be recycled and reused for the same application given the worsening of morphological and mechanical performance [45]. More recently, they assessed up to five processing cycles on the same plasticized PLA through reactive extrusion, but considered combined extrusion/injection cycles instead of compression molding for

reprocessing [46]. Their main observation was that, although reactive extrusion significantly reduced the molar mass of the plasticized PLA due to chain scission reactions induced by free radicals, the mechanical and molecular performance remained almost unaltered after five reprocessing cycles.

Several studies have been published in recent years regarding the recycling of PLA-based bionanocomposites. Among them, the contributions of Beltrán [47], Botta [48], Scaffaro [49], Tesfaye [50], Dhar [51], and Peinado [52] must be highlighted, with all of them containing only the PLA matrix and the nanoparticles. Beltrán et al. evaluated the recycling of PLA/clay (2 wt%) nanocomposites during extrusion/compression and demonstrated that recycled materials, including service life simulation, behave similarly to the virgin ones after one recycling stage regardless of applying a washing step. Better particle dispersion after reprocessing was achieved, which contributed to counterbalancing polymer matrix degradation during recycling [47]. Botta et al. studied the reprocessing of nanocomposites of PLA/graphene nanoplatelets (5 wt%) after five cycles using a single screw extruder and also found higher particle dispersion with a stabilizing effect of the nanoplatelets [48]. This was similar to what was demonstrated by Scaffaro et al. with PLA/hydrotalcite (5 wt%) nanocomposites, who also found the opposite effects of chain scission due to thermo-mechanical degradation caused by five extrusion cycles and the increase in filler dispersion after multiple reprocessing [49]. In this line, Tesfaye et al. prepared and recycled PLA/silk nanocrystals (1 wt%) nanocomposites and applied four reprocessing extrusion cycles, observing that the silk nanocrystals stabilized the mechanical performance after reprocessing [50]. On the other hand, Dhar et al. assessed the preparation and reprocessing of grafted PLA/cellulose nanocrystals (1–3 wt%) during reactive extrusion using dicumyl peroxide as the initiator and demonstrated the utility of grafting for counteracting the consequences of one cycle of mechanical recycling [51]. Finally, Peinado et al. showed the potential reprocessability and recyclability of PLA/nanoclay (3 wt%) nanocomposites with a melt strength enhancer (4 wt%) after up to twenty reprocessing extrusions, which retained mechanical properties regardless of the decrease in the viscosity [52]. Nevertheless, recycling plasticized bionanocomposites has not been reported to date, and given the high number of newly developed PLA-based nanocomposites with plasticizers [23,53,54], the study of the consequences of subsequent processing stages becomes necessary and is indeed the novelty and core of this research.

Altogether, even though promising results on the mechanical reprocessing of biopolymers and bionanocomposites have been achieved, it does not seem easy to close the recycling loop for particular applications such as food packaging, as it is currently applied for other polymers in this sector, as poly(ethylene terephthalate) (PET) [55]. A complementary perspective involves considering the downgrading of materials as an opportunity for applications with lower performance requirements. Indeed, using multiple-processed materials for downgraded applications has been reported as an added-value alternative for biobased polymers, including PLA [36,56,57].

This study aims, therefore, to evaluate the structural and morphological consequences of reprocessing PLA-based bionanocomposites containing PEG as a plasticizer and acetylated NFC as a bio-based nanofiller. A strategy based on the successive sequence of compounding, injection, and compression molding was applied to obtain pellets, dog-bone, and film specimens. The structural and morphological properties of the different materials were thoroughly assessed after each stage in terms of molar mass, crystalline structure, and thermo-oxidative stability. Finally, the performance of bionanocomposites was validated as a proof of concept for the foreseen applications from a downgrading perspective. In detail, the mechanical performance of dog-bone specimens after injection molding was validated, considering a first service life requiring high stability, strength, and resistance. Then, the water immersion performance of thermo-compressed films obtained after the second processing stage was evaluated to assess the contribution of PEG and NFC in the structures with an advanced degree of degradation for a foreseen second service life.

2. Materials and Methods

2.1. Materials and Reagents

Poly(lactide) (PLA) pellets (Grade 4032D) were supplied by NatureWorks LLC (Minnetonka, MN, USA), with a density of 1.24 g/cm^3 and average molar mass in weight (M_w) of 1×10^5 g/mol and D-isomer content of 1.4%. Poly(ethylene glycol) (PEG) from Merck (Darmstadt, Germany) with M_w 1500 g/mol (PEG-1500) and 400 g/mol (PEG-400) were used as plasticizing agents. Nanofibrillated cellulose (NFC) was obtained from Eucalyptus Bleached Kraft Pulp (80% *Eucalyptus globulus* and 20% *Eucalyptus nitens*) in the form of sheets, supplied by CMPC Pulp S.A. Santa Fe Mill (Nacimiento, Chile). Tetrahydrofuran (THF) ($\geq$99.8%) used as solvent and mobile phase during chromatographic analyses was supplied by Scharlau$^{\circledR}$ (Barcelona, Spain) and used without further purification.

2.2. Preparation of Nanofibrillated Cellulose (NFC)

The kraft pulp sheets were processed by grinding until disintegrated fibers with a size of less than 1 cm were obtained. The fibers were then partially acetylated with glacial acetic acid (180 °C, 2 h, solid/liquid ratio 1/20) and recirculated in a laboratory disc refiner operating at 2500 rpm for 40 passes to ensure size reduction and the homogeneity of the NFC. Subsequently, after cooling, the NFC suspension was diluted in heptanol and heated to remove the acetic acid, which has a lower boiling point. Finally, water was added to displace the heptanol from the NFC and separate it by decantation, thus avoiding drying the fibers during these processes. The prepared acetylated NFC fibers have a degree of substitution of 0.52, determined by titration according to Rodrigues Filho et al. [58], and an average width of 30 nm, determined by the intrinsic viscosity according to the model of Albornoz-Palma et al. [59] (parameters: [η] = 1003 mL/g, average length = 8.1 μm). The morphology of the NFC can be appreciated in the scanning electron micrograph in Figure S1 in the Supplementary Materials.

2.3. Compounding, Processing, and Recycling of Bionanocomposites

For the compounding stage of the bionanocomposites, 400 and 1500 g/mol poly(ethylene glycol) (PEG) were first blended with NFC at 120 °C with a DLAB MS-H280-PRO magnetic hot plate (Beijing, China) for 40 min. Subsequently, the PEG/NFC was combined with PLA in a torque rheometer Brabender model 815,653 (Duisburg, Germany) for 5 min at 180 °C and 50 rpm. For the plasticized PLA used as reference, PEG was directly combined with PLA in the torque rheometer at the abovementioned conditions. As for the proportions, 7.5 wt% plasticizer was added with respect to PLA in the blends, and for the bionanocomposites, NFC proportions of 1, 3, and 5 wt% were included, based on the sum of the mass of PLA and PEG. These NFC percentages were precisely selected according to previous literature studies that found agglomeration at nanofiller percentages above 5 wt% [25,26,60,61]. Therefore, the actual proportions of all of the components in the resulting nanocomposites were calculated, as shown in Table 1. For the sake of clarity, the nanocomposite samples were labeled according to the entire numeral of NFC weight percentage.

Table 1. Composition and designation of the samples.

Designation	PLA (wt%)	PEG-400 (wt%)	PEG-1500 (wt%)	NFC (wt%)
PLA	100.00	-	-	-
PLA-400	92.50	7.50	-	-
PLA-400-NFC1	91.59	7.42	-	0.99
PLA-400-NFC3	89.81	7.28	-	2.91
PLA-400-NFC5	88.10	7.14	-	4.76
PLA-1500	92.50	-	7.50	-
PLA-1500-NFC1	91.59	-	7.42	0.99
PLA-1500-NFC3	89.81	-	7.28	2.91
PLA-1500-NFC5	88.10	-	7.14	4.76

Afterward, these compositions were processed through injection molding into Type IV ASTM D638 dog-bone specimens [62] in a mini-injector jet HAAKE MiniJet II (Vreden, Germany) with a preheating stage of 2 min at 190 °C. The temperature of the molds was 55 °C, and the injection and post-pressure were 40 MPa and 30 MPa, respectively.

Subsequently, the dog-bone specimens were cut by hand into ~3 mm diameter pellets and reprocessed into flat rectangle sheets with a thickness of 0.5 ± 0.1 mm through compression molding using a custom-made four-axis hot plate press. Preheating at 190 °C for 10 min was followed by a pressure of 4.9 MPa for 3 min, 7.4 MPa for 3 min, and 9.8 MPa for another 3 min. After compression, the samples were removed from the hot press and cooled at room temperature with pressure to avoid deformation. The processing sequence and the appearance of the obtained specimens are shown in Figure 1.
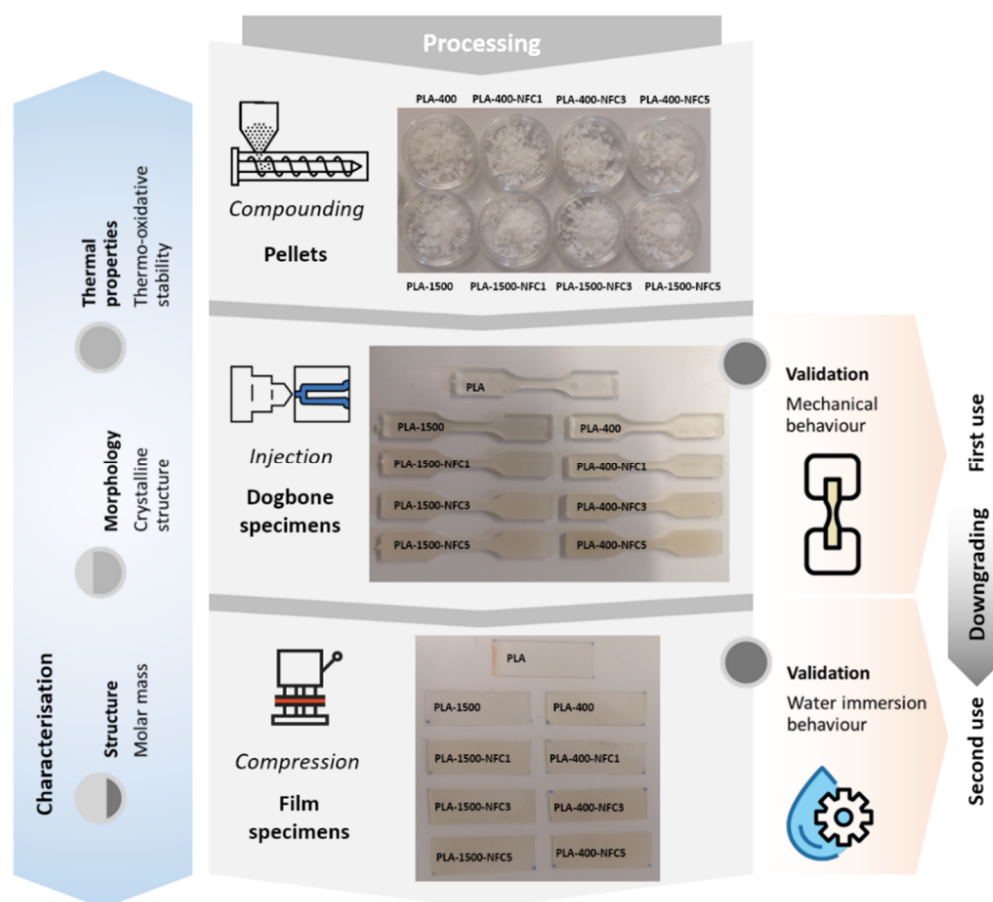

Figure 1. Overall approach of this study, involving the successive processing stages of compounding, injection molding, and compression molding, together with the physico-chemical characterization and validation strategies from a downgrading perspective.

2.4. Gel Permeation Chromatography (GPC)

Gel permeation chromatography was carried out through a Malvern Instruments (Worcestershire, UK) Omnisec Resolve chromatograph, combining an integrated pump, a degasser, an autosampler, and a column oven, along with a Malvern Instruments Omnisec Reveal multi-detector including ultraviolet (UV), refractive index (RI), low- and right-angle light scattering (LALS and RALS), and viscosity (VISC). A monodisperse polystyrene standard with dn/dc of 0.185 was used for calibration. Two columns from Malvern Instruments (T2000 and T4000) were used (300 mm × 8 mm) with tetrahydrofuran (THF) as the mobile phase at a flow rate of 1 mL/min and a column temperature of 35 °C. The samples were dissolved in THF with concentrations of around 2.0 mg/mL and filtered

through 0.45 μm PTFE filters. Two injections per sample (100 μL) were performed, and the obtained data were analyzed using the Omnisec™ v11 software.

2.5. Differential Scanning Calorimetry (DSC)

Calorimetric data were obtained by differential scanning calorimetry using a Mettler Toledo DSC 820 series (Columbus, OH, USA). The samples (4 mg) were placed in aluminum crucibles (40 μL). Three successive heating/cooling/heating segments were applied, with a heating/cooling rate of 10 °C/min between 0 and 200 °C, using N_2 as protective gas at a flow of 50 mL/min. The samples were analyzed in triplicates, and averages and deviations were taken as representatives. The degree of crystallinity (X_c) was calculated through Equation (1), where $\Delta h_m°$ is the value of the melting enthalpy of a perfect crystal of infinite size (93 J/g) [28]; Δh_m is the melting enthalpy; Δh_{cc} is the cold crystallization enthalpy; and f is the fraction weight of PLA in the nanocomposites. The lamellar thickness (l_c) was calculated by applying the Thomson–Gibbs equation (Equation (2)) based on the temperatures associated with the melting transitions [63,64]. In this equation, T_m is the melting peak temperature; T_m^0 is the equilibrium melting temperature of an infinite crystal (480 K); σ_e is the surface free energy of the basal plane where the chains fold (60.89×10^{-3} J/m^2); and Δh_{mV} is the melting enthalpy per volume unit (111.083×10^8 J/m^3) [65].

$$X_c(\%) = \frac{\Delta h_m - \Delta h_{cc}}{f \times \Delta h_m^{\circ}} \times 100 \tag{1}$$

$$l_C(T_m) = \left[\left(1 - \frac{T_m}{T_m^0}\right) \times \frac{\Delta h_{mV}}{2 \times \sigma_e}\right]^{-1} \tag{2}$$

2.6. Thermogravimetric Analysis (TGA)

Thermo-oxidative stability data were obtained using a Mettler Toledo TGA 851 series (Columbus, OH, USA). The samples (4 mg) were introduced into TGA Mettler Toledo perforated alumina crucibles (70 μL) and were analyzed using a dynamic procedure, with a heating rate of 10 °C/min in the temperature range of 25 to 800 °C, under an oxidative atmosphere of O_2 at a flow rate of 50 mL/min. The samples were analyzed in triplicates, and averages and deviations were taken as representatives.

2.7. Field Emission Scanning Electron Microscopy (FE-SEM)

The surface morphology of the cryofracture specimens and the changes after the tensile fracture were analyzed using a Zeiss Ultra 55 field emission scanning electron microscope (FE-SEM) (Oberkochen, Germany). The cryofracture method involved the immersion of the sample in liquid N_2 for 3 min, followed by breakage into two pieces using appropriate forceps. Cryo- and tensile-fractured samples were cut into small pieces, mounted on metal studs, and sputter-coated with Pt for 15 s using a Leica EM MED020 coater (Wetzlar, Germany). The measuring conditions involved a voltage of 1.50 kV and a working distance of 5 mm at 22 °C.

2.8. Tensile Test

Uniaxial tensile tests of the nanocomposites were performed in Type IV dog-bone specimens prepared according to ASTM D638 [62]. A Shimadzu AG-100kNXplus uniaxial test machine was used for the tensile tests with a load cell of 10 kN and a crosshead speed of 1 mm/min. The thickness of the specimens was ~3.2 mm, the length of the grip sections was 10 mm at both ends, and the gauge length was 10 mm. The samples were analyzed in triplicates, and averages and deviations were taken as representatives.

2.9. Water Absorption Studies

The water absorption was evaluated by monitoring the gravimetric change due to the amount of penetrant retained as a function of time, as adopted from the standard EN-ISO

62:2008 [66]. In this study, immersion temperatures of 8, 23, 58, and 70 °C were selected to simulate the conditions of feasible applications of these materials. First, 8 °C was chosen as a typical temperature in a refrigerator for the storage of food packaging. Then, 23 °C represents standard room temperature, which is predominantly used for storing packaging materials and is referred to in the standards EN-ISO 62 [66] and ASTM D570-98 [67]. Next, 58 °C was selected as the usual temperature used for biodegradation studies of PLA [38,68], as described in the standards ASTM D6400-04 [69], ASTM D6868-03 [70], ASTM D5338-11 [71], ASTM D7081-05 [72], DIN EN 13432:2000-12 [73], or ISO 14855-2 [74]. Finally, 70 °C may simulate applications where higher temperatures can occur, such as in automobiles or electronic parts. It also allows seeing the water uptake behavior over the glass transition of PLA in the rubbery state. The immersion at 8 °C was carried out in a refrigerator from Aspes Type 4FAC4858 (Mondragón, Spain), while the temperatures of 23, 58, and 70 °C were achieved in an oven from Heraeus Instruments Type B 12 (Hanau, Germany). The water absorption studies were performed in duplicates, considering two specimens per sample/condition, and averages and deviations were considered as representatives. To measure the mass change, the mass of the dry samples (m_0) was first obtained in a Mettler Toledo AB135-S scale (Columbus, OH, USA). Then, they were placed in glass vials, assuring complete immersion in distilled water at the given temperature. After certain periods, the samples were weighed once the traces of water on the surface (m_1) were removed. The percentage of absorbed water (M_t) was calculated according to Equation (3). With many measurements of M_t, the water absorption profiles were obtained and used to determine the time needed to reach half-saturation ($t_{1/2}$). With this value, the diffusion coefficient (D) in the early stages of immersion was calculated according to Equation (4), where l is the thickness of the film [75]. Furthermore, the solubility coefficient (S) was calculated according to Equation (5), where m_p is the weight of the PLA matrix in the composite, m_s is the weight of the specimen at the equilibrium or peak of water absorption, and m_0 is the initial weight of the specimen before immersion. Finally, the permeability coefficient (P) was obtained according to Equation (6) as a function of solubility and diffusion.

The obtained results were evaluated using main effects plots (MEP) that help determine the isolated impact of the inputs of this study (temperature and composition) on the mentioned outputs (M_s, D, S, and P). By calculating the arithmetic means by adding the numeric values for the respective levels, the influence of a single input can be analyzed, while the influences of the other inputs are cancelled.

$$M_t(\%) = \frac{(m_1 - m_0)}{m_0} \times 100 \tag{3}$$

$$D = \frac{0.01227l^2}{t_{1/2}} \tag{4}$$

$$S = \frac{(m_s - m_0)}{m_p} \tag{5}$$

$$P = D \times S \tag{6}$$

3. Results and Discussion

Figure 1 illustrates the overall approach of this study. In detail, a multiple processing sequence was applied to pure PLA, PEG plasticized PLA, and PLA/PEG/NFC bionanocomposites to ascertain the physico-chemical consequences caused by processing, and evaluate the role and functionality of PEG and NFC along this course. The processing stages involved: (i) compounding in a torque rheometer to formulate pellets, (ii) injection molding to prepare normalized dog-bone specimens, and (iii) compression molding to obtain film-shaped samples. This order was prudently selected to reduce the impact of the processing strategy on the polymer structures, given that compression molding may avoid the contribution of shear forces that have a crucial role during injection molding. Indeed, it has been

demonstrated for PLA that degradation increases during injection in comparison to other melt processing approaches and is more relevant with increasing rotor speed [76].

The structural and morphological consequences caused by processing were characterized in detail by assessing the molar mass, thermal properties, crystalline structure, and thermo-oxidative stability, respectively. Special attention was paid to the contribution of PEG with different molar masses, as well as to the different proportions of NFC. Although properties of polymer materials, especially in thermoplastic-matrix-based composites, are known to decay after successive processing stages, particular applications for each state can be considered. On this subject, the overall end-of-life of a product must be distinguished from the end-of-life of a given material for a particular application. Indeed, using multiple-processed materials for downgraded applications has been reported as an added-value alternative for biobased polymers [56]. Therefore, the resulting bionanocomposites after the injection and compression molding stages were validated according to their particular properties and foreseen applications, signifying the first and second service life, and involving a downgrading perspective.

3.1. Structural and Morphological Consequences of Processing

3.1.1. Molar Mass

The molar mass of polymers is a critical factor in determining other physico-chemical properties, such as thermal, chemical, or mechanical stability [77]. Hence, the consequences of the successive processing stages and the contribution of both PEG and NFC on the molar mass of PLA were first ascertained. Figure 2 plots the obtained Gaussian-like molar mass distributions, which were displaced towards lower values after processing due to mechanical and thermal degradation. The contribution of PEG and NFC after each processing stage was studied in detail with the aid of the average molar mass in number (M_n) and weight (M_w), plotted in Figure 3 and gathered in Table S1.

After compounding, both the average molar mass in the number (M_n) and weight (M_w) of PLA were reduced due to high temperatures and shear stresses in the torque rheometer [26]. This decrease was more significant in the M_w than in the M_n due to the breakage of long PLA chains. The use of low molar mass PEG in PLA-400 resulted in more chain scission in the PLA matrix, together with the possibility of establishing crosslinks with broken PLA chains. Nevertheless, in the PLA-1500, the higher molar mass of PEG slightly buffered the consequences of compounding in terms of molar mass reduction. As for the molar mass distributions, the chain breakage when PEG was incorporated was demonstrated by the low molar mass population with a peak around $\sim 3 \times 10^4$ g/mol. Regarding the role of NFC, it has been reported that it can cause shear effects during compounding and promote more degradation [78–80]; its contribution was non-critical and not perceivable in either the molar mass distributions or the calculated results. Only a minor additional decrease in the molar mass could be detected (<10%), especially in the M_n of PLA-400-NFC nanocomposites.

The subsequent injection molding to obtain dog-bone specimens significantly affected the molar mass. Indeed, distributions moved towards lower values, and a more relevant low-molar mass cue was appreciated, which determined the variation of M_n. A different pattern was found for pure PLA than for blends and nanocomposites. For PLA, M_n and M_w were slightly reduced (14% and 8%), while the molar mass reduction in the plasticized PLA and PLA-PEG-NFC nanocomposites after injection molding was significantly higher (>40% and >24%, respectively). At this point, non-relevant differences according to the molar mass of the PEG could be identified in the molar mass distributions However, a 10–15% reduction was found in the M_n of PLA-400-NFC bionanocomposites caused by NFC. Nevertheless, the influence of the NFC was non-critical and a general tendency correlated to the NFC percentage in the nanocomposites could not be established.
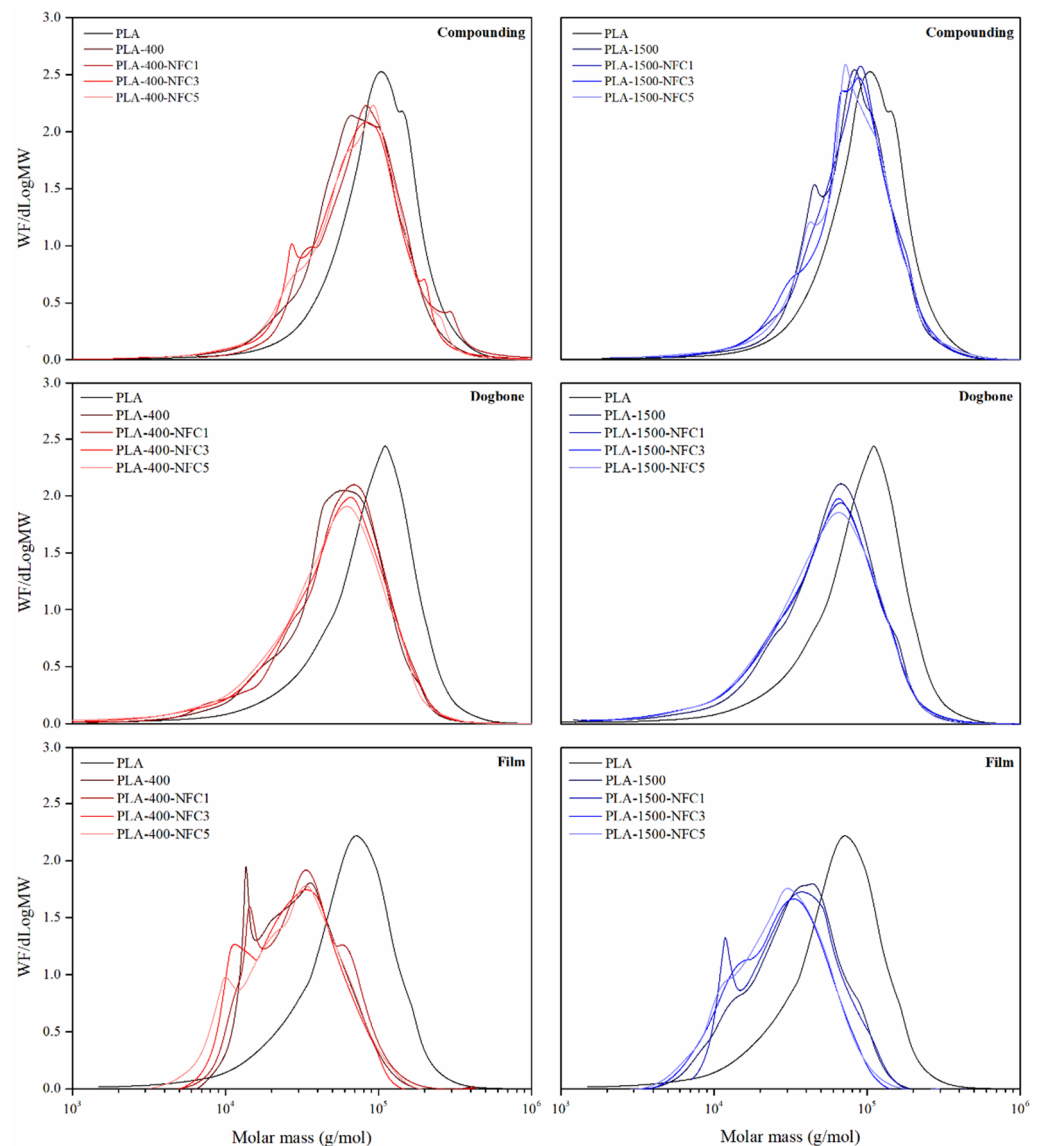
Figure 2. Molar mass distributions of PLA, plasticized PLA-PEG, and PLA-PEG-NFC bionanocomposites after the subsequent stages of compounding, dog-bone, and film specimen preparation.

Finally, the compression molding stage to obtain films correspondingly reduced the molar mass in all of the compositions, but more restrainedly. M_n and M_w were further reduced for PLA (19% and 28%), while for the plasticized PLA-400 and PLA-1500 and bionanocomposites, the molar mass reduction was especially relevant in the M_w (>31%). Apart from the displacement towards lower values, their molar mass distributions also showed a sharp peak at ~10^4 g/mol. This peak is ascribed to the generation of a polymer chain population with lower molar mass due to chain scission caused by the intensive temperature and pressure applied during thermo-compression regardless of the molar mass of PEG. Once more, the contribution of NFC did not significantly affect the molar mass distributions, with variations in the M_n and M_w values lower than 10% in comparison to their PLA-PEG counterparts. Nevertheless, as the NFC content increased, a greater molar mass was identified in the PLA-1500-NFC compositions. As reported before by other authors for other nanofillers, a better dispersion of nanoparticles may be achieved after successive processing stages, with the possibility of having established crosslinking interactions with the matrix and contributing to buffering the degradation rate and stabilizing the molar mass to a greater extent [47–50].
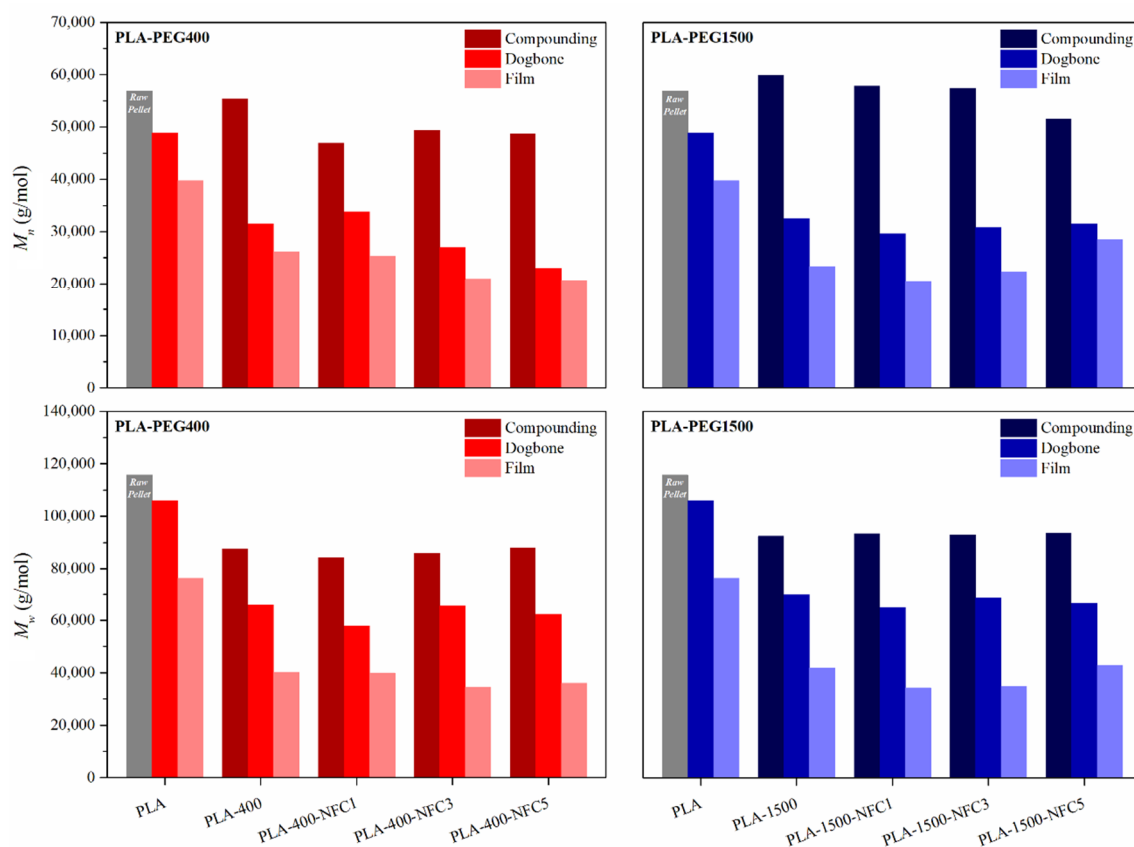
Figure 3. Average molar mass in number (M_n) (up) and weight (M_w) (down) for the PLA-400 (left) and PLA-1500-based bionanocomposites (right) after the subsequent stages of compounding, dog-bone, and film processing stages. A standard deviation below 5% was omitted for the sake of clarity.

Overall, the contribution of the compounding stage was significant in terms of M_w variation, given the preferential degradation of long PLA chains. Then, the injection molding caused global thermo-mechanical degradation due to applying shear forces and temperature that significantly reduced M_w and M_n and involved the most aggressive processing conditions. Afterward, the consequences of the degradation due to the thermo-compression were primarily perceivable in terms of M_w due to heat that caused the generation of a low molar mass population visible in the obtained distributions. In terms of composition, the molar mass of pure PLA was reduced by 30% and 34% for M_n and M_w, respectively, in line with what has been reported in the literature for raw PLA with three reprocessing cycles [34]. In general, the use of PEG enhanced the thermochemical degradation of PLA [45,46]. Although PEG-400 promoted more degradation during the compounding stage for plasticized PLA, the differences after injection and compression molding were non-relevant for the PEG with dissimilar molar mass. At the end of the processing sequence, the M_n and M_w were globally reduced by 53% and 54% for PLA-400 and by 58% and 55% for PLA-1500, respectively. Comparable molar mass reductions were reported in multi-reprocessed plasticized PLA with acrylated PEG [45]. Finally, even though the presence of NFC was non-critical, it seemed to augment degradation in combination with PLA-400, while it contributed to retaining the molar mass when reinforcing PLA-1500 compositions, especially at the highest concentrations (5 wt%).

3.1.2. Thermal Properties and Crystalline Structure

The change in molar mass is widely known to promote variations in the crystalline structure of PLA and, consequently, in the thermal properties. Therefore, calorimetric analyses were carried out during subsequent heating–cooling–heating scans. While the

first heating scan erases the thermal history of the samples and removes the existing crystalline state given by the processing conditions, the controlled cooling scan at a given rate guarantees the creation of a known and identical thermal history for all of the assessed samples. Thus, materials can be intrinsically evaluated in the second heating scan, avoiding the specific effects of processing, storage, or transportation. The thermograms of the first heating and subsequent cooling scans are illustrated in Figures S2 and S3 of the Supplementary Materials. Those of the second heating segment are shown in Figure 4. The glass transition temperature (T_g) measured in the cooling scan, together with the degree of crystallinity (X_c) and the lamellar thickness (l_c) calculated in the second heating scan, were selected as key indicators of the crystalline structure and are plotted in Figure 5 and gathered in Table S1.
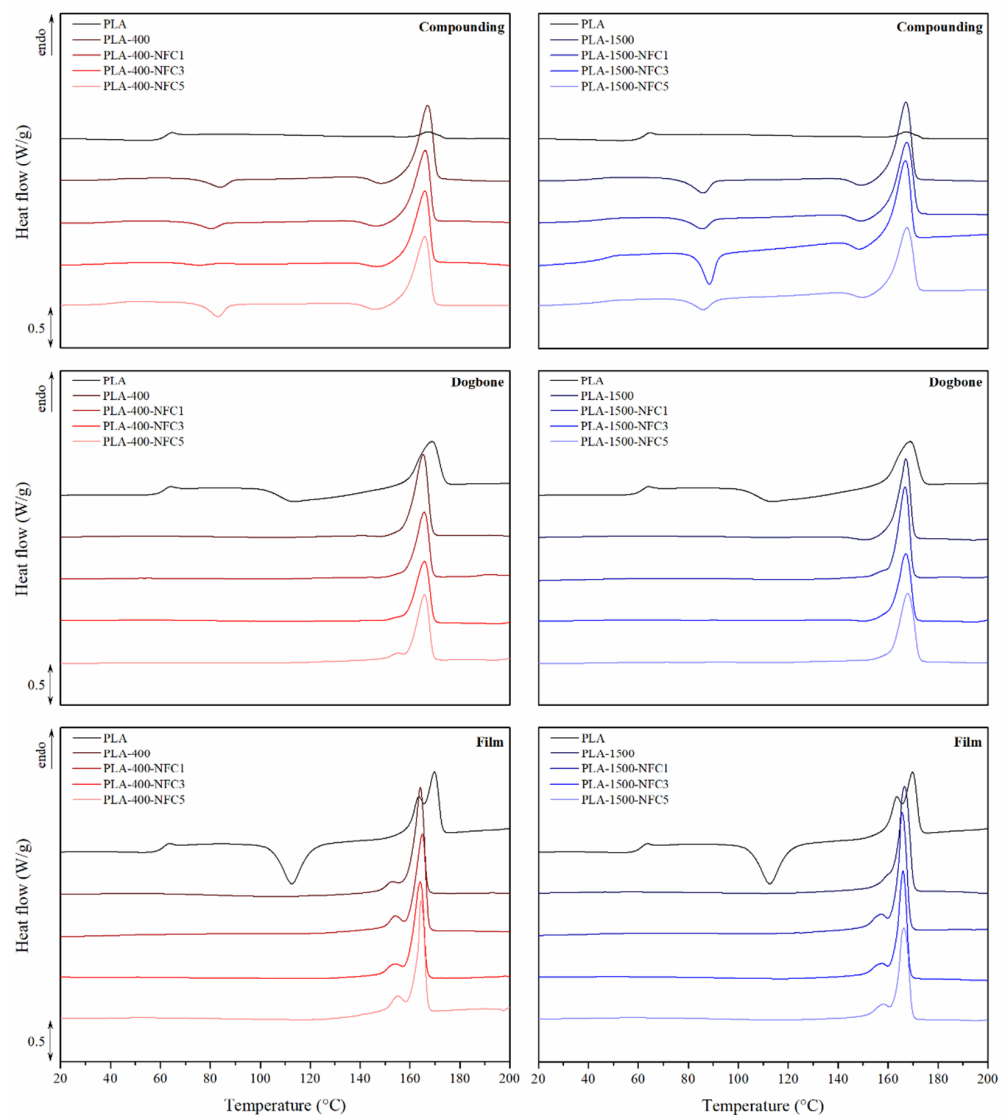

Figure 4. Calorimetric thermograms for the second heating scan of PLA, plasticized PLA-PEG, and PLA-PEG-NFC bionanocomposites after the subsequent stages of compounding, dog-bone, and film specimen preparation.
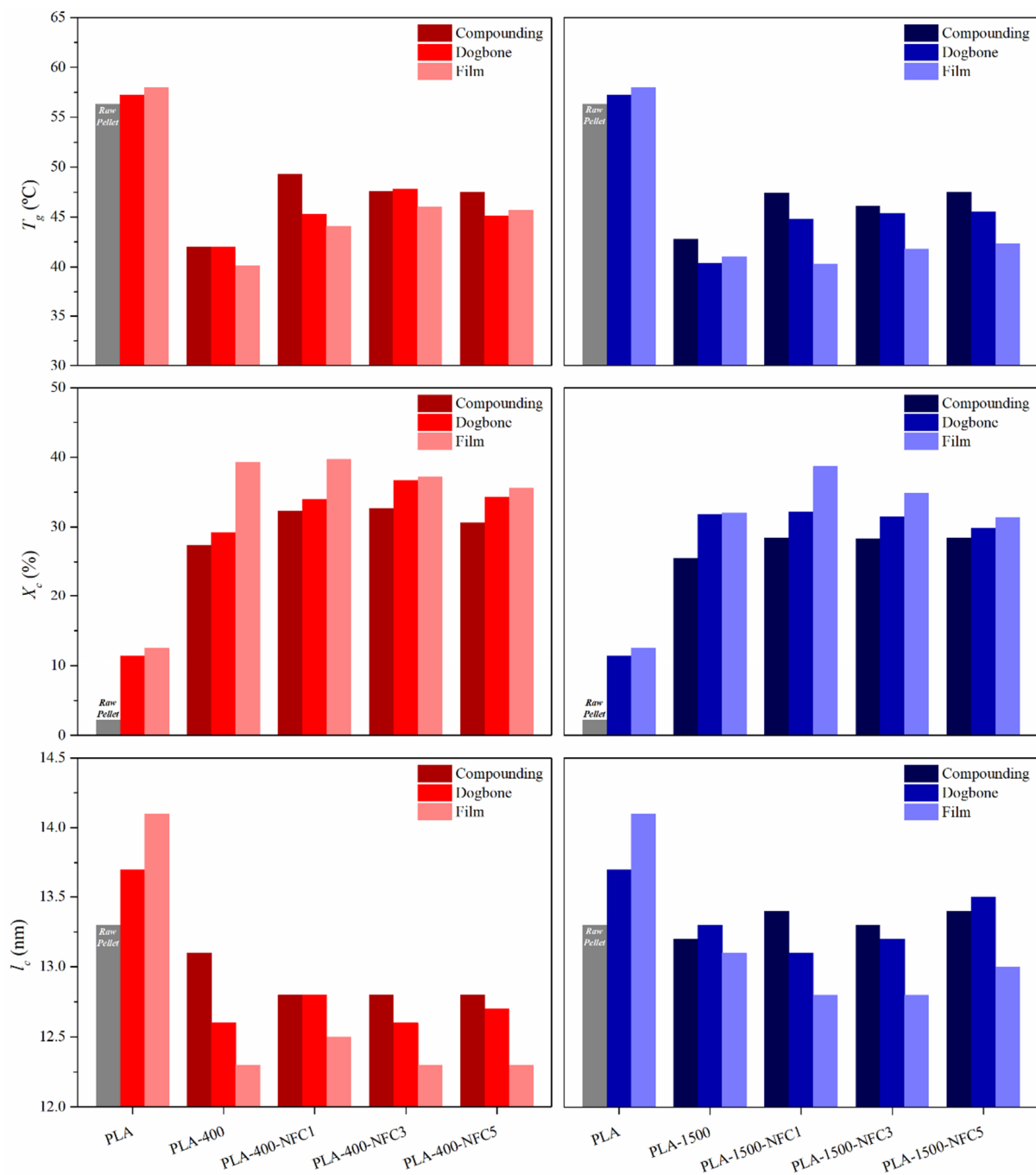
Figure 5. Glass transition temperature (T_g), degree of crystallinity (X_c), and lamellar thickness (l_c) for the bionanocomposites after the subsequent stages of compounding, dog-bone, and film specimen preparation. A standard deviation between 1% and 5% was omitted for the sake of clarity.

Pure PLA pellets showed a glass transition at 56 °C, followed by a small melting peak that resulted in a predominant amorphous structure with a degree of crystallinity of 2% and a lamellar thickness of 13.3 nm. These values are in line with those previously reported for this PLA grade [26,28].

The glass transition temperature of compounded plasticized PLA decreased by 25%, given the plasticizing effect of PEG and chain scission caused by compounding. The T_g of PLA-400 was 42 °C, while that of PLA-1500 was 43 °C. In addition, the thermogram of PLA-PEG blends shows a vanishing of structural relaxation, in line with other studies dealing with plasticized PLA [81–83]. The molecules of PEG may have acted as enhancers

of molecular packing, establishing hydrogen bonding, dipole–dipole physical interactions, or even chemical crosslinks with PLA macromolecules during compounding. As a result, some rigid homogeneous PLA–PLA interphases were replaced by heterogeneous flexible PLA–PEG networks, decreasing the enthalpy and avoiding the perception of structural relaxation. This hypothesis was thoroughly demonstrated in other plasticized polymers [84]. Moreover, the PEG promoted the cold crystallization process at temperatures below 80 °C, given the higher mobility of PLA chains that can rearrange during heating. Finally, an intense melting peak was detected for both plasticized PLAs. The degree of crystallinity increased in the plasticized PLA up to 27% for PLA-400 and 25% for PLA-1500, and the lamellar thickness slightly decreased to 13.1 nm regardless of the molar mass of the PEG. Therefore, more crystals with thinner lamellae were produced in the plasticized PLA [45,46].

The addition of NFC slightly increased the glass transition temperature after compounding compared to their PLA/PEG counterparts, especially for low NFC percentages (1 to 3 wt%). These low percentages of NFC may have assured a good dispersion that increased tortuosity for the mobility of the PLA macromolecules and moved the glass transition toward higher temperatures. As the NFC content increased, the slightly lower effect on the glass transition may suggest the possible agglomeration of the filler, with a minor hinderance to the translational and rotational backbone motions of the PLA chains [85]. The NFC also favored cold crystallization at lower temperatures and influenced the melting event that resulted in a higher crystalline degree. This performance, more relevant for the PLA-400 than the PLA-1500-based compositions, may be ascribed to the nucleating behavior of the nanoparticles [86]. The comprehensive analysis of the degree of crystallinity revealed that, in both PLA-400-NFC and PLA-1500-NFC nanocomposites, a limit concentration for the nucleating function in the range from 1 to 3 wt% of nanoparticles was found. As mentioned before, the agglomeration of NFC at higher percentages may have caused a lower nucleating effect and, therefore, a slightly lower degree of crystallinity. This behavior was in line with different studies in the literature, all referring to a nucleating effect of the nanofillers up to agglomeration [25,26,86,87]. Finally, in terms of lamellar thickness, the contribution of the NFC could be appreciated, especially in the PLA-400-NFC nanocomposites, with a slight reduction of l_c from 13.1 to 12.7 nm due to less crystalline perfection. In the PLA-1500-NFC nanocomposites, the l_c remained around 13.2 nm.

After the injection and compression molding stages, the obtained thermograms and selected key indicators (T_g, X_c, and l_c) were altered in all of the assessed materials with relevant differences as a function of the composition. Pure PLA showed the cold-crystallization transition in the vicinities of 112 °C after injection molding and gained importance and moved to 110 °C after thermo-compression. This performance is strictly related to chain scission during processing and is a sign of degradation. Shorter polymer chains have greater mobility and more ability to rearrange during cold-crystallization. Subsequently, a more relevant melting event was observed in the PLA during heating. Altogether, the crystallinity and lamellar thickness increased from 2% to 12% and 13.3 nm to 14.1 nm, respectively. Particularly after compression molding, the melting transition turned from a unimodal to a bimodal pattern, which may be correlated to distinct crystalline populations, with the lower being less prominent with an l_c of 12.1 nm. This performance, previously reported for reprocessed PLA [34], was accompanied by an increase in the glass transition along the different processing stages from 56 °C to 58 °C. The generation of more crystalline regions with higher lamellar thickness promoted steric hindrance in the amorphous regions, resulting in higher glass transition temperatures.

The inclusion of PEG decreased the glass transition temperature after injection and compression molding. The reduction of the molar mass of PLA that generated oligomers, along with the presence of PEG as a plasticizer, allowed for higher mobility, and therefore the glass transition was displaced towards even lower temperatures from ~42 °C to ~40 °C in both blends. While the cold-crystallization disappeared after dog-bone and film processing, the melting event remained a well-defined transition in all cases, given that the PLA managed to reach its potential crystallinity. Consequently, the degree of

crystallinity significantly increased after reprocessing the PLA-400 from 26% to 39% and less prominently for the PLA-1500 from 25% to 32%. The lamellar thickness decreased in the PLA-400 from 13.1 nm to 12.8, remaining around 13 nm for the PLA-1500 after the subsequent processing stages.

Although injection and compression molding reduced the glass transition of bio-nanocomposites, more significant percentages of NFC contributed to retaining higher T_g. This appreciation can be correlated to better nanoparticle dispersion as a function of the processing stages. The NFC nanoparticles also removed the cold-crystallization phenomenon, increased the degree of crystallinity, and reduced the lamellar thickness after reprocessing. The previously described nucleating behavior for low NFC percentages (1 and 3 wt%) was corroborated in the dog-bone and film specimens, especially regarding the degree of crystallinity, which reached maximum values of nearly 40% for the PLA-400-NFC1 and 39% for the PLA-1500-NFC1 as thermo-compressed films. Furthermore, the melting transition remained as a double-melting peak after compression molding and revealed a minor reduction of the lamellar thickness of the more prominent crystalline population. It also generated a small percentage of a crystalline region with a lamellar thickness of around 10 nm, both in the PLA-400-NFC and PLA-1500-NFC bionanocomposites. Such crystalline domains with lower lamellar thickness may be correlated to the crystallization of low molar mass oligomeric segments shown in the distributions discussed in the previous section.

In summary, the chain scission caused by processing significantly influenced the thermal behavior and crystalline morphology of the bionanocomposites. Although some variances could be observed when considering PEG-400 or PEG-1500, differences were non-critical in the crystalline structure. While signs of improved dispersion of NFC were identified as processing advanced in terms of glass transition, the use of NFC in low percentages enhanced nucleation and crystallization with lower lamellar thickness, with a limit concentration of 1 and 3 wt%.

From a technological perspective, it can be highlighted that the high degrees of crystallinity reached by the blends and bionanocomposites compared to pure PLA after reprocessing suggest that thermal history and processing circumstances, especially the conditions during cooling (10 °C/min in this study), are of high relevance for achieving a crystalline morphology that allows for the desired performance. In this regard, fast cooling procedures during processing may permit an adequate balance between amorphous and crystalline fractions to avoid the fragile performance of such highly crystalline structures.

3.1.3. Thermo-Oxidative Stability

The thermo-oxidative stability of the materials after the different processing stages was also analyzed, as it may bring a complementary view to the study of the molar mass and crystalline morphology. The obtained thermogravimetric thermograms (TG) and derived curves (DTG) are displayed in Figures S4 and S5 of the Supplementary Materials, respectively. These thermograms were assessed in detail in terms of the onset temperature (T_o) and primary decomposition process (T_p) of PLA, which were considered critical parameters for evaluating the consequences of reprocessing, and are reported in Table 2.

Pure PLA revealed a single-stage decomposition process with an onset of around 332 °C. Beyond this point, the weight loss increased, and the decomposition reached its maximum rate at 356 °C and finished at about 370 °C. According to the literature, the starting point for the decomposition of virgin PLA can be related to the loss of end groups from the main chain or ester bond scission [88,89], which ultimately results in the decomposition of the polymer backbone [68]. Finally, a minor step from 400 to 500 °C is due to the subsequent char decomposition [90,91].

Once compounded, the thermo-oxidative decomposition of plasticized PLA-400 and PLA-1500 showed a two-stage profile. The first stage, with a peak temperature of 245 °C and a weight loss of ~7%, may be attributed to the decomposition of PEG, in which the mass percentage virtually matches its expected ratio in the blend [90]. Then, the second and main stage, between 330 °C and 375 °C, involved the principal mass loss due to the

decomposition of the PLA backbone. Although the decomposition of PEG was observed in the blends at lower temperatures, it did not alter the onset and peak temperatures of the main decomposition stage of PLA (T_o and T_p).

Table 2. Thermo-oxidative decomposition parameters for the bionanocomposites after the subsequent compounding stages and dog-bone and film specimen preparation: onset (T_o) and peak (T_p) temperatures. *P* stands for pellet, *C* for compounding, *D* for dog-bone, and *F* for film specimens.

		T_o (°C)	T_p (°C)			T_o (°C)	T_p (°C)
PLA	P	332.1 (±0.6)	355.6 (±1.7)				
	D	333.0 (±2.1)	354.3 (±0.3)				
	F	332.4 (±4.2)	355.9 (±1.8)				
PLA-400	C	330.5 (±1.1)	357.0 (±2.7)	PLA-1500	C	333.0 (±1.3)	358.4 (±1.8)
	D	333.1 (±1.4)	355.0 (±2.4)		D	324.7 (±0.1)	353.5 (±2.6)
	F	326.3 (±2.0)	356.2 (±0.5)		F	326.3 (±0.2)	351.0 (±1.7)
PLA-400-NFC1	C	334.8 (±2.7)	359.9 (±0.6)	PLA-1500-NFC1	C	333.9 (±3.4)	359.6 (±1.1)
	D	334.9 (±1.5)	359.5 (±1.3)		D	331.2 (±1.2)	356.2 (±0.3)
	F	323.5 (±0.7)	355.5 (±0.3)		F	327.4 (±2.0)	356.0 (±1.5)
PLA-400-NFC3	C	337.6 (±1.2)	359.4 (±1.4)	PLA-1500-NFC3	C	334.6 (±1.5)	358.5 (±0.5)
	D	330.8 (±2.6)	357.2 (±0.8)		D	330.0 (±2.2)	352.2 (±3.0)
	F	317.9 (±1.9)	349.6 (±2.9)		F	326.3 (±1.9)	351.9 (±2.7)
PLA-400-NFC5	C	332.8 (±0.4)	357.9 (±0.4)	PLA-1500-NFC5	C	331.3 (±0.3)	356.2 (±0.2)
	D	329.7 (±1.7)	354.5 (±1.1)		D	329.9 (±0.6)	352.2 (±1.3)
	F	319.3 (±1.6)	350.1 (±1.3)		F	330.2 (±1.2)	351.2 (±0.8)

In the compounded nanocomposites, the NFC promoted a general slight displacement of the curve towards higher temperatures, especially for lower percentages of NFC (1 and 3 wt%) in the PLA-400-based materials. All the curves were displaced towards higher temperatures with the addition of low portions of NFC, suggesting higher thermo-oxidative stability. As perceived in previous sections, a key point discussing the stability of the compositions with high NFC percentages may be the nanoparticles' level of dispersion. The agglomeration of the nanofibrillated cellulose in concentrations above 3 wt% may prevent a proper distribution of the filler into the matrix, which impairs improving the thermo-oxidative stability of the bionanocomposites [28]. Nevertheless, as reported by other authors with similar amounts of NFC, only a limited effect of such nanoparticles was found on the thermal stability of PLA nanocomposites [27].

After the subsequent injection and compression molding, the decomposition of PEG in the blends appeared at lower temperatures. However, the presence of NFC in the bionanocomposites buffer this diminution, and even greater temperatures for this first mass loss process ascribed to PEG could be identified. This effect was more relevant in the PLA-400-NFC compositions and can be attributed to the interaction of PEG with the NFC nanoparticles, which was more significant the lower the molar mass of PEG. The successive processing stages moved the onset of decomposition towards lower values. The degraded PLA chains with more presumable carboxylic chain ends may have promoted an earlier onset of decomposition. This behavior could be observed in both the plasticized PLA-400 and PLA-1500 compositions. However, in the bionanocomposites, a noticeable difference was perceived. On the one hand, in PLA-400-NFC, the presence of NFC accentuated the reduction of the T_o. However, in the PLA-1500-NFC nanocomposites, the higher molar mass of PEG seemed to contribute to reducing this fall. Regarding the peak, T_p was moved towards lower temperatures due to the PLA chain scission during processing. While injection molding promoted a more severe reduction of T_p in the PLA-1500 compositions, the PLA-400-based materials were more labile to the stage of compression molding. PEG with higher molar mass and lower plasticizing yield seemed to result in slightly more degradation during injection molding when significant mechanical and thermal stresses

were applied. Finally, the contribution of low percentages of NFC (1 and 3 wt%) buffered the decrease of T_p due to reprocessing compared to their PLA-PEG counterparts. NFC promoted a neat increase of T_p in both PLA-400-NFC and PLA-1500-NFC nanocomposites after injection molding, which was still visible in the compression-molded films, particularly in the PLA-1500-NFC compositions.

Overall, the successive processing stages reduced the thermo-oxidative stability of the bionanocomposites, especially in terms of the onset and peak decomposition temperatures of PLA. It was also pointed out that the use of PEG involved its own degradation process with temperatures in the vicinities of 245 °C that may be considered the limiting temperature during service for these materials. Although using NFC in the plasticized bionanocomposites still resulted in lower thermo-oxidative stability than pure PLA, low percentages (1 and 3 wt%) contributed to retarding the launch of the PEG decomposition and even increased both onset and peak temperatures of PLA. This performance was more relevant the higher the molar mass of PEG.

3.2. Validation of the Bionanocomposites

The validation of polymer materials is essential for corroborating whether the design approach brings functionalities and desired qualities during application [92]. This process is concerned with demonstrating the consistency and completeness of the design concerning the application needs and includes the study of the variation of the product's properties during its service life and, therefore, when exposed to the application environment—real or simulated. According to international norms, standardized quality tests usually delimit these validation procedures.

It has been demonstrated in this study that the successive processing stages promoted significant degradation in all of the analyzed compositions, which was revealed by a noteworthy molar mass reduction, together with changes in the crystalline morphology and thermal properties. In this section, the validation of the bionanocomposites after the first processing cycle of injection molding and the second processing stage of thermo-compression molding was performed from a downgrading perspective. On the one hand, the plasticizing effect of PEG and the reinforcement ability of NFC on the dog-bone injected specimens were validated according to the ASTM D638 Standard Test Method for Tensile Properties of Plastics [62] with a detailed study of the fracture region as a function of the composition. On the other hand, the contribution of the PEG and NFC to the diffusion, sorption, and permeation characteristics was evaluated during the water immersion of the reprocessed thermo-compression film specimens, as described by the EN-ISO 62:2008 Plastics–Determination of water absorption [66].

3.2.1. First Service Life: Mechanical Performance and Fracture Surface of Dog-Bone Specimens

The mechanical validation of the dog-bone specimens was performed through tensile tests in a universal testing machine. The stress–strain diagrams, together with the values of the tensile strength (σ_{max}), the elastic modulus (E), and the elongation at break (ε_{break}), are represented in Figure 6.

For neat PLA, a σ_{max} of 59.3 MPa, an E of 3.51 GPa, and an ε_{break} of 5.6% were measured, all in line with the results reported for this PLA grade, with low flexibility and deformability [88,93]. The PEG-plasticized PLA exhibited a decrease in the σ_{max} with higher ε_{break} [8,81,82]. The reduction of the σ_{max} was around 28% and 19% for the PLA-400 and PLA-1500, respectively. However, a relevant increase in the elongation and, therefore, fracture deformation was registered with the addition of PEG, especially for the PLA-400, with a growth in ε_{break} of nearly 230%. The plasticized PLA-1500 also increased ductility, more restrainedly, with an almost 61% higher elongation. Although the overall deformability increased more the lower the molar mass of PEG, it is interesting to highlight the contribution of the PEG in the elastic region, as can be appreciated in the inset of Figure 6. The stiffness slightly decreased with the addition of PEG given by the lower slope of the elastic deformation region. It is well known that using plasticizing agents such as PEG

endorses flexibility and favors elastic and plastic deformation while decreasing the stiffness and the maximum strength [20,88], as demonstrated in this work.
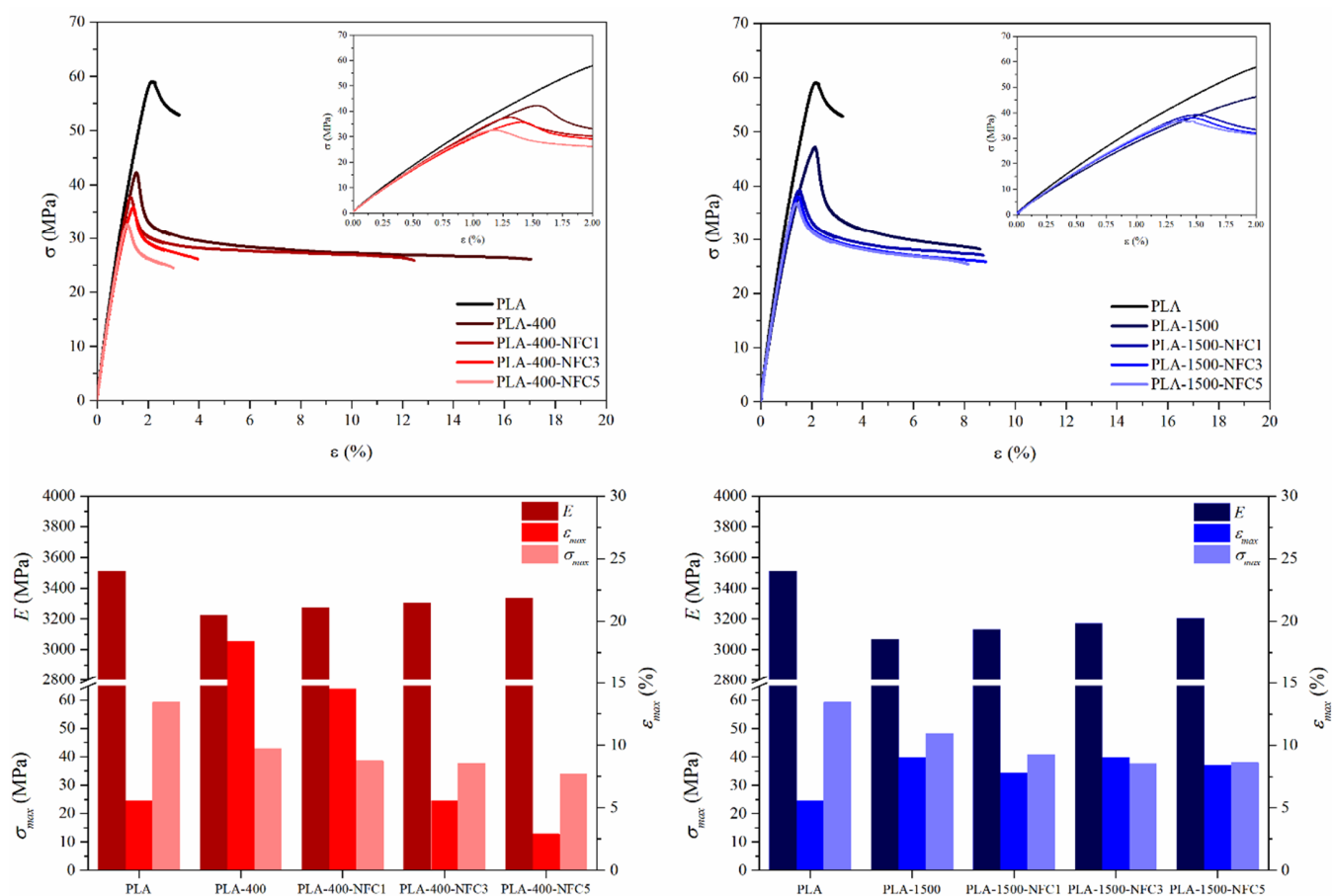

Figure 6. Tensile-stress curves and elastic modulus (E), tensile strength (σ_{max}), elongation at break (ε_{break}) for the dog-bone specimens of PLA, plasticized PLA-PEG, and PLA-PEG-NFC bionanocomposites. A standard deviation between 1% and 6% was omitted for the sake of clarity.

In the bionanocomposites, the addition of NFC generally caused a moderate reduction of σ_{max} concerning their corresponding PLA-PEG counterparts, together with a decrease of the ε_{break} and a slight increase in the E. Although the use of fillers in composite materials is usually accompanied by an improvement in the tensile strength, a minor reduction (<5%) was found in the current study, which may indicate the prevalence of the plasticizing effect of PEG, together with a feasible limited stress transfer across the matrix/filler interphase [27,86,87,94]. This phenomenon may provoke the generation of voids during the tensile test, leading to slightly lower strength values [26]. Complementarily, high NFC contents may be related to forming particle agglomerates with a low aspect ratio, which may affect the tensile strength [95]. Altogether, the variation in the σ_{max} was not censorious, and it may be sacrificed for controlling other parameters such as deformability or rigidity. Regarding the deformation at break, it was more evidence of the contribution of the NFC on the PLA-400-NFC bionanocomposites than those of PLA-1500-NFC. The addition of NFC inhibited the reduction in the stiffness, although the value of pure PLA was not reached. The perceived decrease in the ε_{break} by adding NFC was ascribed to the matrix/filler interaction along with the steric hindrance of the molecular movement of the polymer chains caused by the NFC particles and the changes in the crystalline microstructure that they promoted in the nanocomposites [27,94,95]. This effect was predominant for the samples containing PEG-400. Non-significant differences were noted in the deformation strain caused by the addition of NFC to the PLA-1500 compositions. In this case, the effect of

the PEG-1500 on the elongation at break prevailed above the contribution of the NFC. This behavior is of great importance, as it can be considered that the nanoparticles did not impair the deformability in materials with PEG of high molar mass, but improved, in all cases, the tensile strain of the pure PLA. In terms of elastic modulus, the presence of the NFCs resulted in a linear increase of the material rigidity, especially relevant in the PLA-1500-based bionanocomposites.

At this point, evaluating the microscopic appearance of the surface of the samples both after cryofracture and after the tensile test may give valuable information about the matrix–filler interaction and serve as the baseline for understanding the mechanical performance of these materials. Therefore, field emission scanning microscopy (FE-SEM) was considered, and the obtained micrographs are shown in Figure 7. The cryofractured specimens before the mechanical tests revealed a compact structure without pores or cracks, which suggested a suitable processing strategy for preparing the dog-bone specimens. The frozen samples' typical fragile fracture behavior could be perceived, especially in pure PLA. Although a fragile cryofracture was also found with samples containing PEG, the presence of the plasticizing agent slightly promoted more rugosity [82]. This roughness was more significant for the PLA-1500 than for the PLA-400-based materials, highlighting the contribution of the PEG with higher molar mass to the more substantial increase in the crystallinity of PLA, as revealed in previous sections [81]. In addition, no phase separation was observed, which correlated to good miscibility between the plasticizer and the polymer matrix. For the bionanocomposites containing NFC, the cryofracture surface generally increased in roughness and heterogeneity with the nanofiller percentage, which was particularly relevant for materials based on PLA-1500. The changes mentioned above in the PLA matrix's crystalline microstructure due to the nanofiller's presence may have influenced this behavior.

After the tensile test, the fracture surface of the virgin PLA was almost flat and smooth, indicating a brittle fracture characteristic for this polymer. With the combination of PLA and PEG, signs of ductility could be perceived. However, non-relevant differences were appraised between the plasticized PLA in terms of the molar mass of PEG. The presence of thread-like structures corroborates the plasticizing effect correlated with the growth in the elongation at break. For the case of bionanocomposites containing NFC, the main observation was the presence of high porosity and voids, together with an irregular fracture surface. This was more visible as the NFC content increased and may be related to a partial matrix–filler interaction along with the possible agglomeration of the nanoparticles, especially for high NFC percentages (5 wt%). Furthermore, bigger pores were noted in the nanocomposites with PEG-400 compared with PEG-1500 nanocomposites, according to the slightly lower resistance to fracture and higher elongation at break displayed by the PEG-400-NFC compositions.

Here, it is necessary to remark that both the mechanical and microscopic performances are strictly related to the crystalline morphology of the dog-bone specimens after injection molding, of which calorimetric thermograms of the first heating scan are shown in Figure S2. Therefore, the crystalline structure of such dog-bone specimens is of great importance, and consequently, the degree of crystallinity (X_{c0}) was calculated and is presented in Table 3. Higher crystallinity was found with the addition of PEG and low percentages of NFC (1 wt%). Nevertheless, the higher deformation at break in nanocomposites containing PEG suggested that its plasticizing effect in the amorphous regions prevailed over the generation of crystalline domains. The general higher X_{c0} of the PLA-1500-NFC nanocomposites may explain their lower deformation at break compared to PLA-400-NFC, together with the increase in the rigidity of these materials.

Finally, observing the macroscopic appearance of the fracture region in the dog-bone specimens, it was easy to detect a whitish area formed due to necking during the tensile tests, in which strain-induced crystallization could be visually identified. This behavior was corroborated by analyzing the crystallinity of the close-to-fracture section. The obtained degree of crystallinity of the fracture region ($X_{c\,frac}$) is also presented in Table 3.

In general, unless for pure PLA, a significant increase in the crystallinity degree in the fracture region was found for the plasticized PLA and bionanocomposites. As suggested in previous sections, using PEG may allow the PLA macromolecular chains to flow and rearrange, forming tensile-induced crystalline domains. Moreover, moderated percentages of NFC (1 and 3 wt%) enhanced the crystallization due to its nucleating performance. At the same time, higher amounts of NFC (5 wt%) promoted the lowest variation in the degree of crystallinity after mechanical fracture, probably due to the already mentioned nanofiller agglomeration.
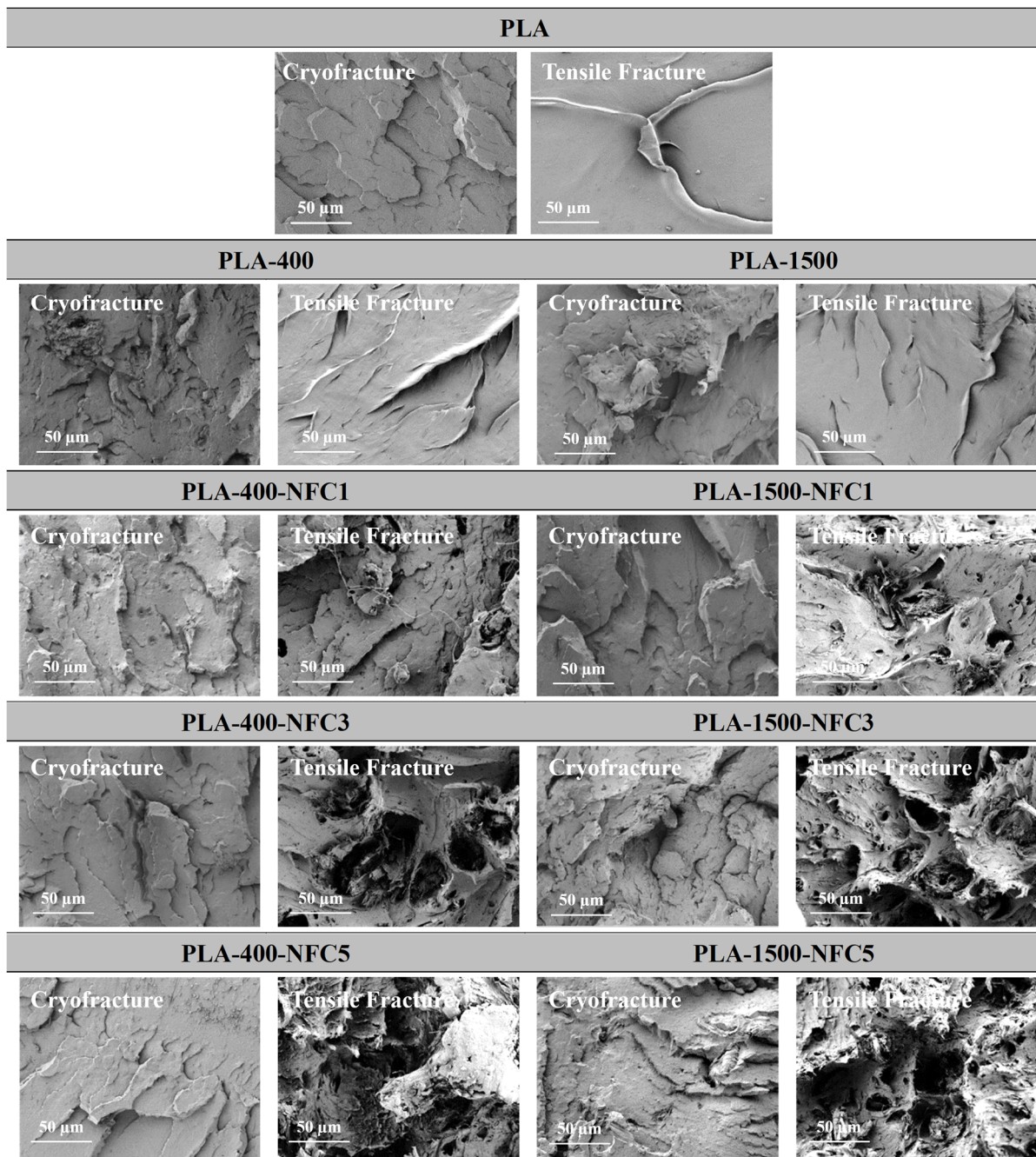
Figure 7. Microscopic appearance of cryofracture surfaces (left) and tensile fracture surfaces (right) of the dog-bone specimens of PLA, plasticized PLA-PEG, and PLA/PEG/NFC bionanocomposites.

Table 3. Degree of crystallinity of dog-bone specimens after processing (X_{c0}) and in the fracture region after the tensile test ($X_{c\,frac}$).

	X_{c0} (%)	$X_{c\,frac}$ (%)
PLA	15.3 ($\pm$2.6)	15.0 ($\pm$4.0)
PLA-400	18.5 ($\pm$0.8)	42.0 ($\pm$2.2)
PLA-400-NFC1	19.1 ($\pm$0.1)	39.8 ($\pm$0.2)
PLA-400-NFC3	15.9 ($\pm$0.5)	37.0 ($\pm$4.9)
PLA-400-NFC5	16.6 ($\pm$1.1)	32.6 ($\pm$3.8)
PLA-1500	20.8 ($\pm$1.4)	40.8 ($\pm$0.6)
PLA-1500-NFC1	25.7 ($\pm$2.6)	42.6 ($\pm$0.8)
PLA-1500-NFC3	20.5 ($\pm$0.2)	36.4 ($\pm$3.5)
PLA-1500-NFC5	20.6 ($\pm$0.3)	34.2 ($\pm$3.8)

3.2.2. Downgraded Second Service Life: Diffusion, Sorption, and Permeation of Water in Film Reprocessed Specimens

The thermo-compressed reprocessed films were validated by assessing their water absorption behavior during immersion at 8, 23, 58, and 70 °C. The water absorption profiles as a function of time are plotted in Figure 8, where the early absorption after immersion and the virtual saturation could be perceived.
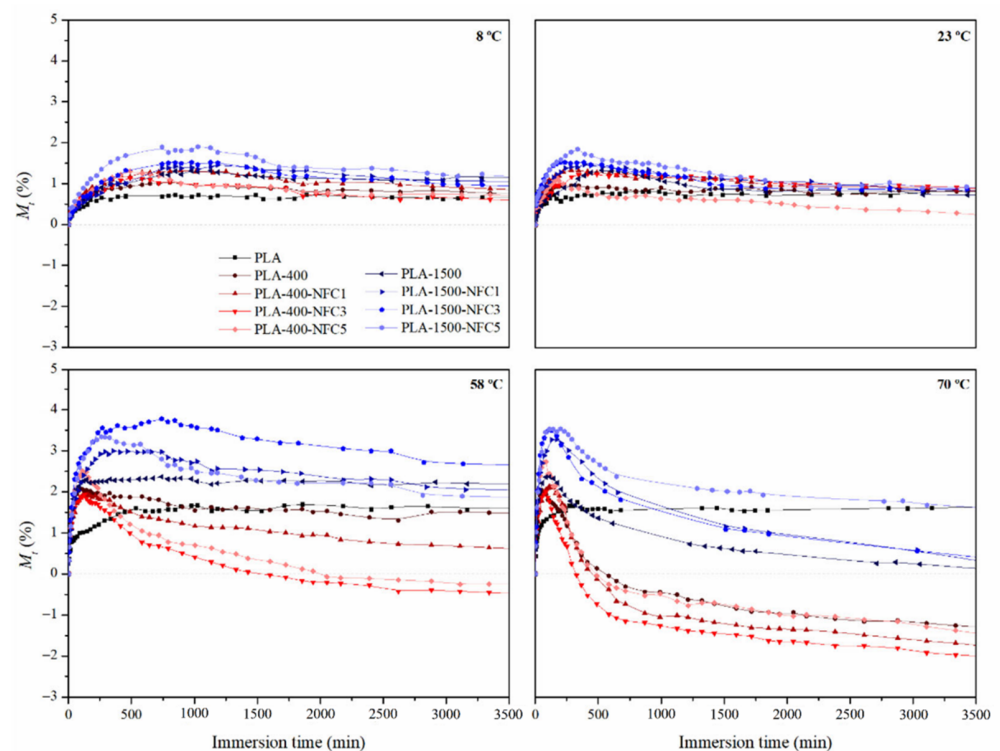
Figure 8. Absorbed percentage of water (M_t) during immersion for the PLA, plasticized PLA-PEG, and PLA-PEG-NFC nanocomposite films at 8, 23, 58, and 70 °C.

The absorption profiles for neat PLA in the initial immersion stage looked similar for all of the temperatures. First, the percentage of absorbed water (M_t) increased fast and almost linearly, followed by a less intense non-linear growth until the curve reached saturation, involving a classic Fickian performance [96–101]. The mass of the PLA increased by ~0.75% through the immersion in water at 8 and 23 °C, while at 58 and 70 °C, the mass augmented up to ~1.5% at saturation. Therefore, as expected, higher temperatures increased the water uptake of the PLA. The curves of the plasticized PLA-400 and PLA-1500 showed a more relevant increase in mass compared to neat PLA due to the hydrophilic nature of PEG, with

multiple hydroxyl groups in its structure. The higher molar mass of the PEG involved more water absorption. The more cohesive and entangled the system, the more PLA-1500 can swell and increase the water uptake ability. For the bionanocomposites, a trend towards even higher water uptakes was observed when the NFC content increased, especially at the lowest temperatures. Although the NFC in this study was acetylated for improving dispersion and may result in a hydrophobic behavior, it can still have hydroxyl groups available to attract water to its surface. Moreover, interfacial defects and nanovoids in the confluence of the matrix and nanoparticles may endorse new free-volume sites for water penetration.

Interestingly, the plasticized PLA-PEG and the PLA-PEG-NFC bionanocomposites started losing mass after the initial water absorption, especially at higher temperatures, representing a non-Fickian behavior. Therefore, the initial fast water absorption was followed by progressive mass loss, which resulted in a peaking phenomenon. The curves at 8 and 23 °C reach a steady equilibrium after the mass loss, while the curves of the temperatures of 58 and 70 °C continue to fall, even reaching a neat mass loss of 2% for the most extreme temperature. Although it was accentuated in the nanocomposites, highlighting the contribution of the nanoparticles, the occurrence of this behavior in the plasticized PLA-400 and PLA-1500 without NFC suggested that the presence of PEG played a crucial role in this subject. Incorporating hydrophilic plasticizers can contribute to increased swelling and later allow soluble parts to be released from the matrix. The release of PEG domains due to the kinetic motion of the plasticized PLA matrix at temperatures above their T_g is the most reasonable circumstance, as found by other authors in PLA-based systems when immersed in water [102–104]. Predictably, this phenomenon was more significant for the PEG with lower molar mass in the PLA-400 blend than for the longer PEG segments in the PLA-1500 compositions [103]. Complementarily, with water-soluble PEG, the dissolution of low-molar mass PLA segments generated during processing or hydrolysis during immersion together with nanoparticles may also have to be considered feasible [99,101,102]. Altogether, this observation suggests a limited degree of chemical crosslinking of PEG and PLA after the applied processing sequence, highlighting the establishment of physical interactions between the matrix and the plasticizer.

Given the confluence of several factors on the water uptake of these materials, i.e., temperature and composition, a detailed investigation was carried out. For this purpose, the water mass absorbed at saturation (M_s), the diffusion coefficient (D), the solubility coefficient (S), and the permeability coefficient (P) were calculated. The obtained values for every material at each immersion temperature are summarized in Figure S6 of the Supplementary Materials. It should be noted that for virgin PLA, the M_s involved the mass at equilibrium, while for the blends and bionanocomposites, the maximum of the curve was taken as the value of M_s. All of the M_s, S, D, and P values were statistically analyzed to determine the global influence of the immersion temperature and the composition. Figures 9 and 10 represent the main effects plot (MEP) for temperature and composition, respectively. The means of the obtained values for each selected temperature and composition were calculated and visually compared.

Figure 9 shows the temperature contribution to the water immersion performance, where a pairwise grouping for the M_s and S values can be observed. While the polymer chains maintain the morphology and structure determined by processing below the glass transition in the glassy state (8 and 23 °C), they gain mobility and start moving above the glass transition in the rubbery state (58 and 70 °C), doubling the values of M_s and S. This movement allows the chains to rearrange themselves, resulting in more free volume in the matrix, more penetration sites for water molecules, and higher absorbed quantities of water. Other studies also found this temperature dependency for the water absorption of PLA-plasticized materials [99,102,105]. The diffusivity (D) and permeability (P) coefficients also show sensitivity toward the immersion temperature. Higher temperatures generally result in stronger vibrations of the water molecules and more free void volume due to increased segmental motion, resulting in a higher diffusion coefficient [97,106].

Although the permeation coefficient (*P*) combines the solubility coefficient (*S*) and diffusion coefficient (*D*), it is predominantly influenced by the diffusivity and shows a similar temperature dependency, showing an exponential growth pattern when the temperature of the environment increases [107].
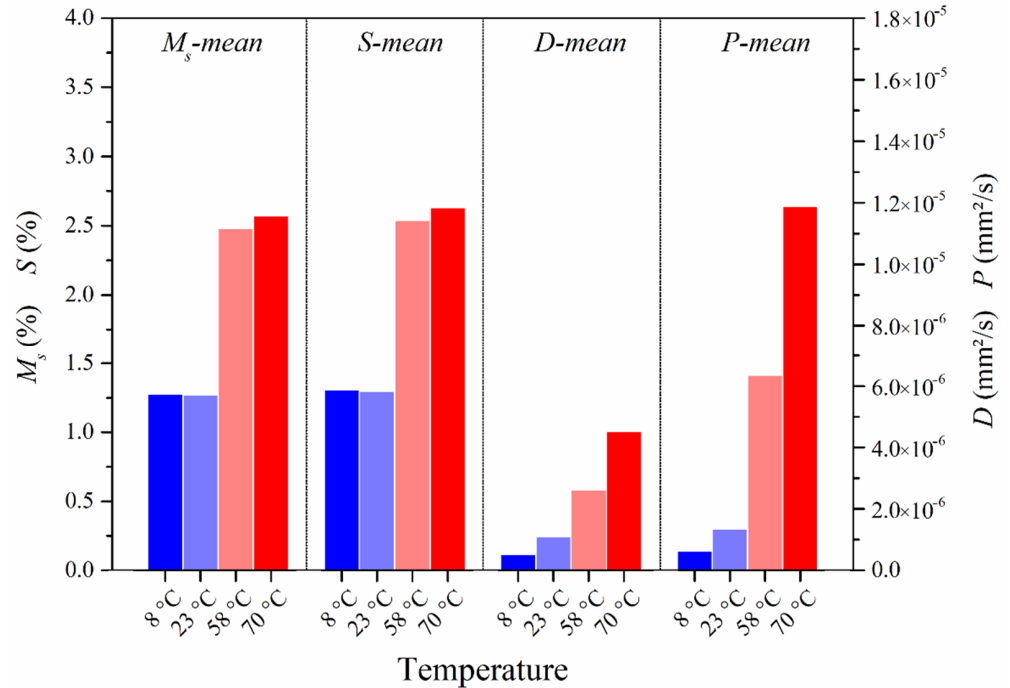

Figure 9. Influence of the immersion temperature on the mean of absorbed mass at saturation (M_s), solubility coefficient (*S*), diffusion coefficient (*D*), and permeability coefficient (*P*) of the PLA, plasticized PLA-PEG, and PLA-PEG-NFC nanocomposite materials.
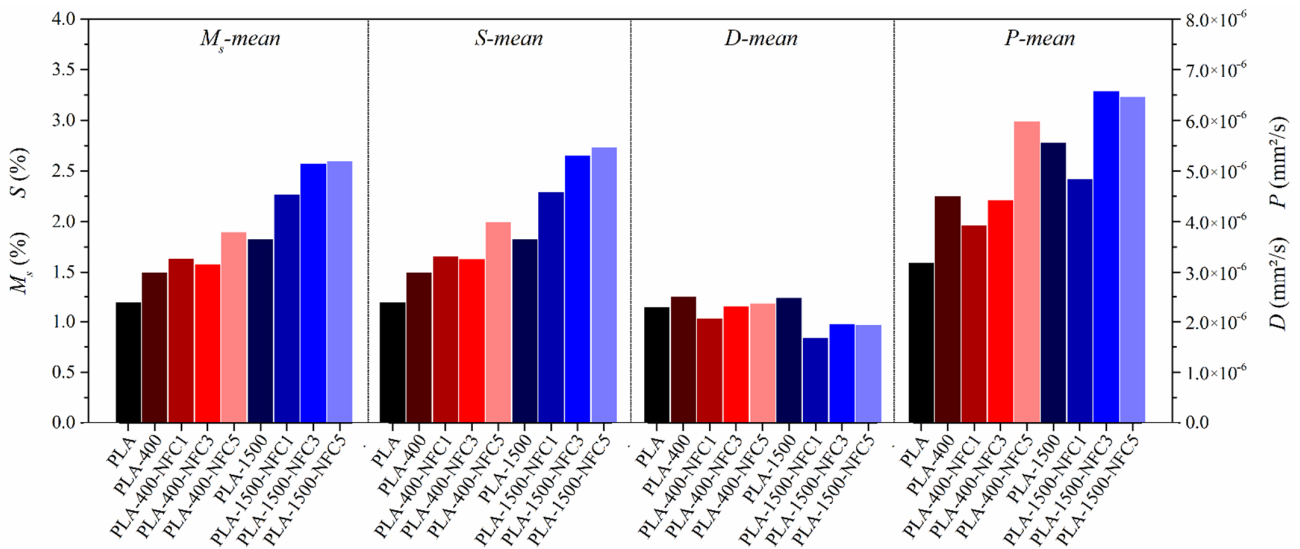
Figure 10. Influence of the composition on the mean of absorbed mass at saturation (M_s), solubility coefficient (*S*), diffusion coefficient (*D*), and permeability coefficient (*P*) of the PLA, plasticized PLA/PEG, and PLA/PEG/NFC nanocomposite materials.

Finally, the influence of the PEG plasticizing agent and NFC nanoparticles on the nature of water absorption was investigated. Figure 10 plots the mean values for the M_s, *D*, *S*, and *P*, in which an evident influence of the compositions on the water uptake performance could be found. Compared to neat PLA, the M_s and *S* were higher for the

plasticized PLA-400 and PLA-1500 due to the hydrophilic nature of PEG, together with its plasticizing effect [105,106]. Furthermore, NFC seems to have contributed to the composites attracting more water and can result in swelling, microcracking, and capillarity phenomena in the matrix [108,109]. This offers new possible penetration pathways resulting in higher amounts of water absorbed by the composite [105,109–111].

A similar pattern was found in the plasticized materials regarding the diffusion (D) and permeation (P) coefficients. Both D and P increased in the blends with the presence of PEG. In this regard, the higher the molar mass of PEG, the greater D and P were obtained. Therefore, higher hydrophilicity due to plasticizer was correlated to faster water penetration and permeation. However, lower diffusion coefficients can be observed with the presence of NFC in all cases. This reduction was more accentuated for low NFC percentages (1%) and the PEG of higher molar mass. Although the hydrophilic character of the NFC may indicate an increase in the diffusivity, the generation of a more cohesive and entangled structure, especially in the PLA-1500, with better dispersed low percentages of NFC nanoparticles and a crystalline structure with greater lamellar thickness resulted in a more tortuous advance of the penetrant and, consequently, lower diffusion coefficients.

Even though a more cohesive structure in the bionanocomposites modulated diffusivity, they still revealed more water incorporation and solubility coefficients, probably due to the possible generation of micro- and nanovoids in the matrix–filler interphase during immersion that subsequently resulted in higher permeability. However, the exception for the 1 and 3 wt% of NFC in the PLA-400-NFC and the 1 wt% in the PLA-1500-NFC materials must be highlighted. Such low percentages of nanoparticles effectively reduced the films' overall permeability through a lower diffusivity and stability during immersion.

Overall, it can be said that higher temperatures favored the absorption of water and the diffusivity, solubility, and permeability. The presence of PEG as a plasticizer and NFC as a reinforcement nanofiller also increases the absorbed mass of water at saturation and the solubility coefficient. Finally, the diffusivity and permeability increased with PEG, but they could be modulated with small percentages of NFC nanoparticles.

4. Conclusions

The possibilities of reprocessing polylactide (PLA)-based bionanocomposites with nanofibrillated cellulose (NFC) and plasticized with poly(ethylene glycol) (PEG) were demonstrated, assuming relevant polymer degradation and encouraging their use for downgraded applications after reprocessing.

Plasticizing PLA with PEG promoted more significant degradation during the first and second processing stages. Low-molar mass PEG slightly accentuated thermo-mechanical degradation during compounding, while non-relevant differences between PEG-400 and PEG-1500 were found after injection molding and thermo-compression. In terms of crystalline morphology, the plasticizing effect of PEG and accentuated chain scission enhanced the mobility of the PLA to form crystalline domains, emphasized for compositions with PEG with lower molar mass. The technological limitation must also be considered due to the thermo-oxidative decomposition of PEG at temperatures much lower than that of PLA. The presence of NFC in the bionanocomposites was not critical for the chain scission of PLA during processing. Complementarily, the NFC acted as a nucleating agent favoring crystallization with a limited concentration for the nucleating function in the range from 1 to 3 wt% of NFC. The evaluation of the thermal properties, especially after reprocessing, pointed out the necessity of controlling the cooling stage, as it may determine the final crystalline structure and, therefore, the specimens' performance.

The mechanical validation of the injection-molded dog-bone specimens for a first service life demonstrated the contribution of PEG as a plasticizer to increase ductility and reduce tensile strength and tensile modulus. It was more relevant the lower the molar mass of PEG, especially at a low concentration of NFC. The addition of NFC reduced the drop in the stiffness caused by PEG, still offering higher elongation at break than pure PLA. The

increasing porosity and an uneven fracture surface for high NFC contents (5 wt%) may be related to the agglomeration of the nanoparticles during processing.

The exploration of reprocessed compression-molded films for a second service life during water immersion revealed the contribution of high temperatures to the absorption of water, diffusivity, solubility, and permeability. PEG and NFC increased the absorbed water and the solubility coefficient. The integrity of the plasticized films was compromised due to the release of PEG domains during immersion in the rubbery state at high temperatures (58 and 70 °C), especially for the PEG with lower molar mass. The role of NFC was demonstrated to modulate diffusivity in all of the compositions, but only small percentages of nanoparticles (1 and 3 wt%) were able to moderate permeability.

Altogether, although reprocessing can cause significant degradation, these bionanocomposites showed promise to be sustainable candidates for food packaging or agricultural applications where modulated mechanical or water contact behaviors are required. Their renewable origin, functionality, and material valorization possibilities will open new possibilities for spreading the use of these green composites.

References

1. Farah, S.; Anderson, D.G.; Langer, R. Physical and Mechanical Properties of PLA, and Their Functions in Widespread Applications—A Comprehensive Review. *Adv. Drug. Deliv. Rev.* **2016**, *107*, 367–392. [CrossRef] [PubMed]
2. Ngo, T.-D. Biobased and Biodegradable Polymers Nanocomposites. In *Handbook of Nanomaterials and Nanocomposites for Energy and Environmental Applications*; Springer: Berlin/Heidelberg, Germany, 2021; pp. 1–28. [CrossRef]
3. Kfoury, G.; Raquez, J.M.; Hassouna, F.; Odent, J.; Toniazzo, V.; Ruch, D.; Dubois, P. Recent Advances in High Performance Poly(Lactide): From "Green" Plasticization to Super-Tough Materials via (Reactive) Compounding. *Front. Chem.* **2013**, *1*, 32. [CrossRef] [PubMed]
4. Hamad, K.; Kaseem, M.; Ayyoob, M.; Joo, J.; Deri, F. Polylactic Acid Blends: The Future of Green, Light and Tough. *Prog. Polym. Sci.* **2018**, *85*, 83–127. [CrossRef]
5. Sun, G.; Chan, C.M. The Effects of the Low-Molecular-Weight Component on Banded Spherulites of Poly(l-Lactic Acid). *Colloid. Polym. Sci.* **2013**, *291*, 1495–1501. [CrossRef]
6. Ljungberg, N. Tributyl Citrate Oligomers as Plasticizers for Poly (Lactic Acid): Thermo-Mechanical Film Properties and Aging. *Polymer* **2003**, *44*, 7679–7688. [CrossRef]
7. Ljungberg, N. The Effects of Plasticizers on the Dynamic Mechanical and Thermal Properties of Poly(Lactic Acid). *J. Appl. Polym. Sci.* **2002**, *86*, 1227–1234. [CrossRef]
8. Baiardo, M.; Frisoni, G.; Scandola, M.; Rimelen, M.; Lips, D.; Ruffieux, K.; Wintermantel, E. Thermal and Mechanical Properties of Plasticized Poly(L-Lactic Acid). *J. Appl. Polym. Sci.* **2003**, *90*, 1731–1738. [CrossRef]
9. Sepúlveda, F.A.; Rivera, F.; Loyo, C.; Canales, D.; Moreno-Serna, V.; Benavente, R.; Rivas, L.M.; Ulloa, M.T.; Gil-Castell, O.; Ribes-Greus, A.; et al. Poly (Lactic Acid)/D-Limonene/ZnO Bio-Nanocomposites with Antimicrobial Properties. *J. Appl. Polym. Sci.* **2022**, *139*, 51542. [CrossRef]
10. Brüster, B.; Adjoua, Y.O.; Dieden, R.; Grysan, P.; Federico, C.E.; Berthé, V.; Addiego, F. Plasticization of Polylactide with Myrcene and Limonene as Bio-Based Plasticizers: Conventional vs. Reactive Extrusion. *Polymers* **2019**, *11*, 1363. [CrossRef] [PubMed]
11. Yang, Y.; Xiong, Z.; Zhang, L.; Tang, Z.; Zhang, R.; Zhu, J. Isosorbide Dioctoate as a "Green" Plasticizer for Poly(Lactic Acid). *Mater. Des.* **2016**, *91*, 262–268. [CrossRef]
12. Ojijo, V.; Sinha Ray, S.; Sadiku, R. Toughening of Biodegradable Polylactide/Poly(Butylene Succinate- Co -Adipate) Blends via in Situ Reactive Compatibilization. *ACS. Appl. Mater. Interfaces.* **2013**, *5*, 4266–4276. [CrossRef] [PubMed]
13. Ren, Z.; Dong, L.; Yang, Y. Dynamic Mechanical and Thermal Properties of Plasticized Poly(Lactic Acid). *J. Appl. Polym. Sci.* **2006**, *101*, 1583–1590. [CrossRef]
14. Maiza, M.; Benaniba, M.T.; Quintard, G.; Massardier-Nageotte, V. Biobased Additive Plasticizing Polylactic Acid (PLA). *Polímeros* **2015**, *25*, 581–590. [CrossRef]
15. Zhao, X.; Liu, J.; Li, J.; Liang, X.; Zhou, W.; Peng, S. Strategies and Techniques for Improving Heat Resistance and Mechanical Performances of Poly(Lactic Acid) (PLA) Biodegradable Materials. *Int. J. Biol. Macromol.* **2022**, *218*, 115–134. [CrossRef]
16. Greco, A.; Ferrari, F. Thermal Behavior of PLA Plasticized by Commercial and Cardanol-Derived Plasticizers and the Effect on the Mechanical Properties. *J. Anal. Calorim.* **2021**, *146*, 131–141. [CrossRef]
17. Younes, H.; Cohn, D. Phase Separation in Poly(Ethylene Glycol)/Poly(Lactic Acid) Blends. *Eur. Polym. J.* **1988**, *24*, 765–773. [CrossRef]
18. Hu, Y. Crystallization and Phase Separation in Blends of High Stereoregular Poly(Lactide) with Poly(Ethylene Glycol). *Polymer* **2003**, *44*, 5681–5689. [CrossRef]
19. Hu, Y.; Rogunova, M.; Topolkaraev, V.; Hiltner, A.; Baer, E. Aging of Poly(Lactide)/Poly(Ethylene Glycol) Blends. Part 1. Poly(Lactide) with Low Stereoregularity. *Polymer* **2003**, *44*, 5701–5710. [CrossRef]
20. Jacobsen, S.; Fritz, H.G. Plasticizing Polylactide? The Effect of Different Plasticizers on the Mechanical Properties. *Polym. Eng. Sci.* **1999**, *39*, 1303–1310. [CrossRef]
21. Pillin, I.; Montrelay, N.; Grohens, Y. Thermo-Mechanical Characterization of Plasticized PLA: Is the Miscibility the Only Significant Factor? *Polymer* **2006**, *47*, 4676–4682. [CrossRef]
22. Sanyang, M.S.; Jawaid, M. *Bio-Based Polymers and Nanocomposites*; Springer International Publishing: Cham, Germany, 2019; ISBN 978-3-030-05824-1.
23. Banerjee, R.; Ray, S.S. An Overview of the Recent Advances in Polylactide-Based Sustainable Nanocomposites. *Polym. Eng. Sci.* **2021**, *61*, 617–649. [CrossRef]
24. Vatansever, E.; Arslan, D.; Nofar, M. Polylactide Cellulose-Based Nanocomposites. *Int. J. Biol. Macromol.* **2019**, *137*, 912–938. [CrossRef]
25. Raisipour-Shirazi, A.; Ahmadi, Z.; Garmabi, H. Polylactic Acid Nanocomposites Toughened with Nanofibrillated Cellulose: Microstructure, Thermal, and Mechanical Properties. *Iran. Polym. J.* **2018**, *27*, 785–794. [CrossRef]
26. Perić, M.; Putz, R.; Paulik, C. Influence of Nanofibrillated Cellulose on the Mechanical and Thermal Properties of Poly(Lactic Acid). *Eur. Polym. J.* **2019**, *114*, 426–433. [CrossRef]
27. Mao, J.; Tang, Y.; Zhao, R.; Zhou, Y.; Wang, Z. Preparation of Nanofibrillated Cellulose and Application in Reinforced PLA/Starch Nanocomposite Film. *J. Polym. Env.* **2019**, *27*, 728–738. [CrossRef]
28. Perić, M.; Putz, R.; Paulik, C. 3D-Printed Pla Filaments Reinforced with Nanofibrillated Cellulose. *J. Renew. Mater.* **2020**, *8*, 759–772. [CrossRef]

29. Gil-Castell, O.; Reyes-Contreras, P.; Barra, P.A.; Mendonça, R.T.; Carrillo-Varela, I.; Badia, J.D.; Serra, A.; Ribes-Greus, A. The Role of Eucalyptus Species on the Structural and Thermal Performance of Cellulose Nanocrystals (CNCs) Isolated by Acid Hydrolysis. *Polymers* **2022**, *14*, 423. [CrossRef]

30. Li, T.; Chen, C.; Brozena, A.H.; Zhu, J.Y.; Xu, L.; Driemeier, C.; Dai, J.; Rojas, O.J.; Isogai, A.; Wågberg, L.; et al. Developing Fibrillated Cellulose as a Sustainable Technological Material. *Nature* **2021**, *590*, 47–56. [CrossRef]

31. Sugawara, E.; Nikaido, H. *Polylactic Acid*; Sin, B.S.T.L.T., Ed.; Elsevier: Amsterdam, The Netherlands, 2019; ISBN 9780128144725.

32. Akbar, M.U.; Rehman, F.U.; Ibrahim, M.; Barikani, M.; Mohammadi, M.; Sobhani, H.; Mohammadi, A.; Farrukh, M.A. Processing Methods of Bionanocomposites. In *Bionanocomposites: Green Synthesis and Applications*; Elsevier: Amsterdam, The Netherlands, 2020; pp. 87–104; ISBN 9780128167519.

33. Badia, J.D.; Gil-Castell, Ó.; Teruel-Juanes, R.; Ribes-Greus, A. Recycling of Polylactide. *Ref. Modul. Mater. Sci. Mater. Eng.* **2019**, *2*, 282–295. [CrossRef]

34. Badia, J.D.; Strömberg, E.; Karlsson, S.; Ribes-Greus, A. Material Valorisation of Amorphous Polylactide. Influence of Thermo-Mechanical Degradation on the Morphology, Segmental Dynamics, Thermal and Mechanical Performance. *Polym. Degrad. Stab.* **2012**, *97*, 670–678. [CrossRef]

35. Badia, J.D.; Monreal, L.; Sáenz de Juano-Arbona, V.; Ribes-Greus, A.; Monreal-Mengual, L.; Sáenz de Juano, V.; Ribes-Greus, A. Dielectric Spectroscopy of Reprocessed Polylactide. *Polym. Degrad. Stab.* **2014**, *107*, 21–27. [CrossRef]

36. Badia, J.D.; Ribes-Greus, A. Mechanical Recycling of Polylactide, Upgrading Trends and Combination of Valorization Techniques. *Eur. Polym. J.* **2016**, *84*, 22–39. [CrossRef]

37. Gil-Castell, O.; Badia, J.D.; Ribes-Greus, A. Suitability of Blends from Virgin and Reprocessed Polylactide: Performance and Energy Valorization Kinetics. *J. Renew. Mater.* **2018**, *6*, 370–382. [CrossRef]

38. Gil-Castell, O.; Badia, J.D.; Ingles-Mascaros, S.; Teruel-Juanes, R.; Serra, A.; Ribes-Greus, A. Polylactide-Based Self-Reinforced Composites Biodegradation: Individual and Combined Influence of Temperature, Water and Compost. *Polym. Degrad. Stab.* **2018**, *158*, 40–51. [CrossRef]

39. Dreier, J.; Brütting, C.; Ruckdäschel, H.; Altstädt, V.; Bonten, C. Investigation of the Thermal and Hydrolytic Degradation of Polylactide during Autoclave Foaming. *Polymers* **2021**, *13*, 2624. [CrossRef]

40. Cosate de Andrade, M.F.; Fonseca, G.; Morales, A.R.; Mei, L.H.I. Mechanical Recycling Simulation of Polylactide Using a Chain Extender. *Adv. Polym. Technol.* **2018**, *37*, 2053–2060. [CrossRef]

41. Benvenuta-Tapia, J.J.; Vivaldo-Lima, E. Reduction of Molar Mass Loss and Enhancement of Thermal and Rheological Properties of Recycled Poly(Lactic Acid) by Using Chain Extenders Obtained from RAFT Chemistry. *React. Funct. Polym.* **2020**, *153*, 104628. [CrossRef]

42. Kfoury, G.; Hassouna, F.; Raquez, J.M.; Toniazzo, V.; Ruch, D.; Dubois, P. Tunable and Durable Toughening of Polylactide Materials Via Reactive Extrusion. *Macromol. Mater. Eng.* **2014**, *299*, 583–595. [CrossRef]

43. Scaffaro, R.; Morreale, M.; Mirabella, F.; La Mantia, F.P. Preparation and Recycling of Plasticized PLA. *Macromol. Mater. Eng.* **2011**, *296*, 141–150. [CrossRef]

44. Pascual-Jose, B.; Badia, J.D.; Múgica, A.; Addiego, F.; Müller, A.J.; Ribes-Greus, A. Analysis of Plasticization and Reprocessing Effects on the Segmental Cooperativity of Polylactide by Dielectric Thermal Spectroscopy. *Polymer* **2021**, *223*, 123701. [CrossRef]

45. Brüster, B.; Addiego, F.; Hassouna, F.; Ruch, D.; Raquez, J.M.; Dubois, P. Thermo-Mechanical Degradation of Plasticized Poly(Lactide) after Multiple Reprocessing to Simulate Recycling: Multi-Scale Analysis and Underlying Mechanisms. *Polym. Degrad. Stab.* **2016**, *131*, 132–144. [CrossRef]

46. Brüster, B.; Montesinos, A.; Reumaux, P.; Pérez-Camargo, R.A.; Mugica, A.; Zubitur, M.; Müller, A.J.; Dubois, P.; Addiego, F. Crystallization Kinetics of Polylactide: Reactive Plasticization and Reprocessing Effects. *Polym. Degrad. Stab.* **2018**, *148*, 56–66. [CrossRef]

47. Beltrán, F.R.; Ortega, E.; Solvoll, A.M.; Lorenzo, V.; de la Orden, M.U.; Martínez Urreaga, J. Effects of Aging and Different Mechanical Recycling Processes on the Structure and Properties of Poly(Lactic Acid)-Clay Nanocomposites. *J. Polym. Env.* **2018**, *26*, 2142–2152. [CrossRef]

48. Botta, L.; Scaffaro, R.; Sutera, F.; Mistretta, M. Reprocessing of PLA/Graphene Nanoplatelets Nanocomposites. *Polymers* **2017**, *10*, 18. [CrossRef]

49. Scaffaro, R.; Sutera, F.; Mistretta, M.C.; Botta, L.; La Mantia, F.P. Structure-Properties Relationships in Melt Reprocessed PLA/Hydrotalcites Nanocomposites. *Express. Polym. Lett.* **2017**, *11*, 555–564. [CrossRef]

50. Tesfaye, M.; Patwa, R.; Kommadath, R.; Kotecha, P.; Katiyar, V. Silk Nanocrystals Stabilized Melt Extruded Poly (Lactic Acid) Nanocomposite Films: Effect of Recycling on Thermal Degradation Kinetics and Optimization Studies. *Thermochim. Acta* **2016**, *643*, 41–52. [CrossRef]

51. Dhar, P.; Tarafder, D.; Kumar, A.; Katiyar, V. Thermally Recyclable Polylactic Acid/Cellulose Nanocrystal Films through Reactive Extrusion Process. *Polymer* **2016**, *87*, 268–282. [CrossRef]

52. Peinado, V.; Castell, P.; García, L.; Fernández, A. Effect of Extrusion on the Mechanical and Rheological Properties of a Reinforced Poly(Lactic Acid): Reprocessing and Recycling of Biobased Materials. *Materials* **2015**, *8*, 7106–7117. [CrossRef]

53. Sharif, A.; Mondal, S.; Hoque, M.E. Polylactic Acid (PLA)-Based Nanocomposites: Processing and Properties. In *Bio-Based Polymers and Nanocomposites: Preparation, Processing, Properties & Performance*; Springer: Berlin/Heidelberg, Germany, 2019; pp. 233–254. [CrossRef]

54. Raquez, J.-M.; Habibi, Y.; Murariu, M.; Dubois, P. Polylactide (PLA)-Based Nanocomposites. *Prog. Polym. Sci.* **2013**, *38*, 1504–1542. [CrossRef]

55. Dedieu, I.; Peyron, S.; Gontard, N.; Aouf, C. The Thermo-Mechanical Recyclability Potential of Biodegradable Biopolyesters: Perspectives and Limits for Food Packaging Application. *Polym. Test.* **2022**, *111*, 107620. [CrossRef]

56. Badia, J.D.; Gil-Castell, O.; Ribes-Greus, A. Long-Term Properties and End-of-Life of Polymers from Renewable Resources. *Polym. Degrad. Stab.* **2017**, *137*, 35–57. [CrossRef]

57. Lamberti, F.M.; Román-Ramírez, L.A.; Wood, J. Recycling of Bioplastics: Routes and Benefits. *J. Polym. Environ.* **2020**, *28*, 2551–2571. [CrossRef]

58. Filho, G.R.; Monteiro, D.S.; da Silva Meireles, C.; de Assunção, R.M.N.; Cerqueira, D.A.; Barud, H.S.; Ribeiro, S.J.L.; Messadeq, Y. Synthesis and Characterization of Cellulose Acetate Produced from Recycled Newspaper. *Carbohydr. Polym.* **2008**, *73*, 74–82. [CrossRef]

59. Albornoz-Palma, G.; Betancourt, F.; Mendonça, R.T.; Chinga-Carrasco, G.; Pereira, M. Relationship between Rheological and Morphological Characteristics of Cellulose Nanofibrils in Dilute Dispersions. *Carbohydr. Polym.* **2020**, *230*, 115588. [CrossRef] [PubMed]

60. Yasim-Anuar, T.A.T.; Ariffin, H.; Norrrahim, M.N.F.; Hassan, M.A.; Andou, Y.; Tsukegi, T.; Nishida, H. Well-Dispersed Cellulose Nanofiber in Low Density Polyethylene Nanocomposite by Liquid-Assisted Extrusion. *Polymers* **2020**, *12*, 927. [CrossRef] [PubMed]

61. Abdulkhani, A.; Hosseinzadeh, J.; Ashori, A.; Dadashi, S.; Takzare, Z. Preparation and Characterization of Modified Cellulose Nanofibers Reinforced Polylactic Acid Nanocomposite. *Polym. Test.* **2014**, *35*, 73–79. [CrossRef]

62. *ASTM D638*; Standard Test Method for Tensile Properties of Plastics. American Society for Testing and Materials (ASTM): West Conshohocken, PA, USA, 2014; Volume 8.

63. Lauritzen, J.I.; Hoffman, J.D. Formation of Polymer Crystals with Folded Chains from Dilute Solution. *J. Chem. Phys.* **1959**, *31*, 1680–1681. [CrossRef]

64. Hoffman, J.D.; Lauritzen, J.I., Jr. Crystallization of Bulk Polymers With Chain Folding: Theory of Growth of Lamellar Spherulites. *J. Res. Natl. Bur. Stand.-A. Phys. Chem.* **1961**, *65*, 1961. [CrossRef]

65. Vasanthakumari, R.; Pennings, A.J. Crystallization Kinetics of Poly(l-Lactic Acid). *Polymers* **1983**, *24*, 175–178. [CrossRef]

66. *ISO 62:2008*; Plastics—Determination of Water Absorption. International Organisation for Standarisation (ISO): Geneva, Switzerland, 2008.

67. *ASTM D570-98*; Standard Test Method for Water Absorption of Plastics. American Society for Testing and Materials (ASTM): West Conshohocken, PA, USA, 2018.

68. Gil-Castell, O.; Andres-Puche, R.; Dominguez, E.; Verdejo, E.; Monreal, L.; Ribes-Greus, A. Influence of Substrate and Temperature on the Biodegradation of Polyester-Based Materials: Polylactide and Poly(3-Hydroxybutyrate-Co-3-Hydroxyhexanoate) as Model Cases. *Polym. Degrad. Stab.* **2020**, *180*, 109288. [CrossRef]

69. *ASTM D6400-04*; Standard Specification for Compostable Plastics. American Society for Testing and Materials (ASTM): West Conshohocken, PA, USA, 2004.

70. *ASTM D6868-03*; Standard Specification for Biodegradable Plastics Used as Coatings on Paper and Other Compostbale Substrates. American Society for Testing and Materials (ASTM): West Conshohocken, PA, USA, 2003.

71. *ASTM D5338-11*; Standard Test Method for Determining Aerobic Biodegradation of Plastic Materials under Controlled Composting Conditions. American Society for Testing and Materials (ASTM): West Conshohocken, PA, USA, 2011.

72. *ASTM D7081-05*; Standard Specification for Non-Floating Biodegradable Plastics in the Marine Environment. American Society for Testing and Materials (ASTM): West Conshohocken, PA, USA, 2005.

73. *DIN EN 13432:2000-12*; Packaging Requirements for Packaging Recoverable through Composting and Biodegradation Test Scheme and Evaluation Criteria for the Final Acceptance of Packaging. Deutsches Institut für Normung (DIN): Berlin, Germany, 2010.

74. *ISO 14855-2:2018*; Determination of the Ultimate Aerobic Biodegradability of Plastic Materials under Controlled Composting Conditions. International Organisation for Standarisation (ISO): Geneva, Switzerland, 2018.

75. Neogi, P. *Diffusion in Polymers*; Marcel Dekker: New York, NY, USA, 1996; Volume 32, ISBN 082479530X.

76. Le Marec, P.E.; Ferry, L.; Quantin, J.-C.; Bénézet, J.-C.; Bonfils, F.; Guilbert, S.; Bergeret, A. Influence of Melt Processing Conditions on Poly(Lactic Acid) Degradation: Molar Mass Distribution and Crystallization. *Polym. Degrad. Stab.* **2014**, *110*, 353–363. [CrossRef]

77. Dragostin, O.; Profire, L. *Molecular Weight of Polymers Used in Biomedical Applications*, 1st ed.; Tanzi, S.F.M.C., Ed.; Elsevier Ltd.: Amsterdam, The Netherlands, 2017; ISBN 9780081007372.

78. Arrieta, M.P.P.; Fortunati, E.; Dominici, F.; Rayón, E.; López, J.; Kenny, J.M.M. PLA-PHB/Cellulose Based Films: Mechanical, Barrier and Disintegration Properties. *Polym. Degrad. Stab.* **2014**, *107*, 139–149. [CrossRef]

79. Beltrán, F.R.; Arrieta, M.P.; Gaspar, G.; de la Orden, M.U.; Urreaga, J.M. Effect of Iignocellulosic Nanoparticles Extracted from Yerba Mate (Ilex Paraguariensis) on the Structural, Thermal, Optical and Barrier Properties of Mechanically Recycled Poly(Lactic Acid). *Polymers* **2020**, *12*, 1690. [CrossRef]

80. Way, C.; Dean, K.; Wu, D.Y.; Palombo, E. Biodegradation of Sequentially Surface Treated Lignocellulose Reinforced Polylactic Acid Composites: Carbon Dioxide Evolution and Morphology. *Polym. Degrad. Stab.* **2012**, *97*, 430–438. [CrossRef]

81. Arias, V.; Höglund, A.; Odelius, K.; Albertsson, A.C. Polylactides with "Green" Plasticizers: Influence of Isomer Composition. *J. Appl. Polym. Sci.* **2013**, *130*, 2962–2970. [CrossRef]

82. Sungsanit, K.; Kao, N.; Bhattacharya, S.N. Properties of Linear Poly(Lactic Acid)/Polyethylene Glycol Blends. *Polym. Eng. Sci.* **2012**, *52*, 108–116. [CrossRef]

83. Dobircau, L.; Delpouve, N.; Herbinet, R.; Domenek, S.; Le Pluart, L.; Delbreilh, L.; Ducruet, V.; Dargent, E. Molecular Mobility and Physical Ageing of Plasticized Poly(Lactide). *Polym. Eng. Sci.* **2015**, *55*, 858–865. [CrossRef]

84. Díaz-Calderón, P.; MacNaughtan, B.; Hill, S.; Mitchell, J.; Enrione, J. Reduction of Enthalpy Relaxation in Gelatine Films by Addition of Polyols. *Int. J. Biol. Macromol.* **2018**, *109*, 634–638. [CrossRef]

85. Habibi, Y.; Dufresne, A. Highly Filled Bionanocomposites from Functionalized Polysaccharide Nanocrystals. *Biomacromolecules* **2008**, *9*, 1974–1980. [CrossRef]

86. Almasi, H.; Ghanbarzadeh, B.; Dehghannya, J.; Entezami, A.A.; Asl, A.K. Novel Nanocomposites Based on Fatty Acid Modified Cellulose Nanofibers/Poly(Lactic Acid): Morphological and Physical Properties. *Food. Packag. Shelf. Life.* **2015**, *5*, 21–31. [CrossRef]

87. Fujisawa, S.; Saito, T.; Kimura, S.; Iwata, T.; Isogai, A. Surface Engineering of Ultrafine Cellulose Nanofibrils toward Polymer Nanocomposite Materials. *Biomacromolecules* **2013**, *14*, 1541–1546. [CrossRef] [PubMed]

88. Barkoula, N.M.; Alcock, B.; Cabrera, N.O.; Peijs, T. Flame-Retardancy Properties of Intumescent Ammonium Poly(Phosphate) and Mineral Filler Magnesium Hydroxide in Combination with Graphene. *Polym. Polym. Compos.* **2008**, *16*, 101–113. [CrossRef]

89. Badia, J.D.; Santonja-Blasco, L.; Martínez-Felipe, A.; Ribes-Greus, A.; Martínez-Felipe, A.; Ribes-Greus, A. Reprocessed Polylactide: Studies of Thermo-Oxidative Decomposition. *Bioresour. Technol.* **2012**, *114*, 622–628. [CrossRef] [PubMed]

90. Mohapatra, A.K.; Mohanty, S.; Nayak, S.K. Effect of PEG on PLA/PEG Blend and Its Nanocomposites: A Study of Thermo-Mechanical and Morphological Characterization. *Polym. Compos.* **2014**, *35*, 283–293. [CrossRef]

91. Khoo, R.Z.; Ismail, H.; Chow, W.S. Thermal and Morphological Properties of Poly (Lactic Acid)/Nanocellulose Nanocomposites. *Procedia. Chem.* **2016**, *19*, 788–794. [CrossRef]

92. CQE. Academy Design Verification & Validation for Quality Engineers. Available online: http://www.cqeacademy.com/cqe-body-of-knowledge/product-process-design/ (accessed on 1 July 2022).

93. Park, S.H.; Lee, S.G.; Kim, S.H. Isothermal Crystallization Behavior and Mechanical Properties of Polylactide/Carbon Nanotube Nanocomposites. *Compos. Part. A Appl. Sci. Manuf.* **2013**, *46*, 11–18. [CrossRef]

94. Qu, P.; Gao, Y.; Wu, G.F.; Zhang, L.P. Nanocomposites of Poly(Lactic Acid) Reinforced with Cellulose Nanofibrils. *Bioresources* **2010**, *5*, 1811–1823. [CrossRef]

95. Zaaba, N.F.; Jaafar, M.; Ismail, H. Tensile and Morphological Properties of Nanocrystalline Cellulose and Nanofibrillated Cellulose Reinforced PLA Bionanocomposites: A Review. *Polym. Eng. Sci.* **2021**, *61*, 22–38. [CrossRef]

96. Berthé, V.; Ferry, L.; Bénézet, J.C.; Bergeret, A. Ageing of Different Biodegradable Polyesters Blends Mechanical and Hygrothermal Behavior. *Polym. Degrad. Stab.* **2010**, *95*, 262–269. [CrossRef]

97. Badia, J.D.; Santonja-Blasco, L.; Martínez-Felipe, A.; Ribes-Greus, A. Hygrothermal Ageing of Reprocessed Polylactide. *Polym. Degrad. Stab.* **2012**, *97*, 1881–1890. [CrossRef]

98. Gil-Castell, O.; Badia, J.D.; Kittikorn, T.; Strömberg, E.; Ek, M.; Karlsson, S.; Ribes-Greus, A.; Strömberg, E.; Ek, M.; Karlsson, S.; et al. Impact of Hydrothermal Ageing on the Thermal Stability, Morphology and Viscoelastic Performance of PLA/Sisal Biocomposites. *Polym. Degrad. Stab.* **2016**, *132*, 87–96. [CrossRef]

99. Ndazi, B.S.; Karlsson, S. Characterization of Hydrolytic Degradation of Polylactic Acid/Rice Hulls Composites in Water at Different Temperatures. *Express. Polym. Lett.* **2011**, *5*, 119–131. [CrossRef]

100. Le Duigou, A.; Davies, P.; Baley, C. Seawater Ageing of Flax/Poly(Lactic Acid) Biocomposites. *Polym. Degrad. Stab.* **2009**, *94*, 1151–1162. [CrossRef]

101. Yew, G.H.; Mohd Yusof, A.M.; Mohd Ishak, Z.A.; Ishiaku, U.S. Water Absorption and Enzymatic Degradation of Poly(Lactic Acid)/Rice Starch Composites. *Polym. Degrad. Stab.* **2005**, *90*, 488–500. [CrossRef]

102. Hrib, J.; Sirc, J.; Hobzova, R.; Hampejsova, Z.; Bosakova, Z.; Munzarova, M.; Michalek, J. Nanofibers for Drug Delivery—Incorporation and Release of Model Molecules, Influence of Molecular Weight and Polymer Structure. *Beilstein. J. Nanotechnol.* **2015**, *6*, 1939–1945. [CrossRef]

103. Moradkhannejhad, L.; Abdouss, M.; Nikfarjam, N.; Shahriari, M.H.; Heidary, V. The Effect of Molecular Weight and Content of PEG on In Vitro Drug Release of Electrospun Curcumin Loaded PLA/PEG Nanofibers. *J. Drug. Deliv. Sci. Technol.* **2020**, *56*, 101554. [CrossRef]

104. Yu, H.Y.; Wang, C.; Abdalkarim, S.Y.H. Cellulose Nanocrystals/Polyethylene Glycol as Bifunctional Reinforcing/Compatibilizing Agents in Poly(Lactic Acid) Nanofibers for Controlling Long-Term in Vitro Drug Release. *Cellulose* **2017**, *24*, 4461–4477. [CrossRef]

105. Leu, Y.Y.; Chow, W.S. Kinetics of Water Absorption and Thermal Properties of Poly(Lactic Acid)/Organomontmorillonite/Poly (Ethylene Glycol) Nanocomposites. *J. Vinyl. Addit. Technol.* **2011**, *17*, 40–47. [CrossRef]

106. Norazlina, H.; Hadi, A.A.; Qurni, A.U.; Amri, M.; Mashelmie, S.; Kamal, Y. Effects of Multi-Walled Carbon Nanotubes (MWCNTs) on the Degradation Behavior of Plasticized PLA Nanocomposites. *Polym. Bull.* **2019**, *76*, 1453–1469. [CrossRef]

107. Tang, C.Y.; Chen, D.Z.; Yue, T.M.; Chan, K.C.; Tsui, C.P.; Yu, P.H.F. Water Absorption and Solubility of PHBHV/HA Nanocomposites. *Compos. Sci. Technol.* **2008**, *68*, 1927–1934. [CrossRef]

108. Joseph, P.V.; Rabello, M.S.; Mattoso, L.H.C.; Joseph, K.; Thomas, S. Environmental Effects on the Degradation Behaviour of Sisal Fibre Reinforced Polypropylene Composites. *Compos. Sci. Technol.* **2002**, *62*, 1357–1372. [CrossRef]

109. Azwa, Z.N.; Yousif, B.F.; Manalo, A.C.; Karunasena, W. A Review on the Degradability of Polymeric Composites Based on Natural Fibres. *Mater. Des.* **2013**, *47*, 424–442. [CrossRef]

110. Dhakal, H.N.; Zhang, Z.Y.; Richardson, M.O.W. Effect of Water Absorption on the Mechanical Properties of Hemp Fibre Reinforced Unsaturated Polyester Composites. *Compos. Sci. Technol.* **2007**, *67*, 1674–1683. [CrossRef]

111. Gil-Castell, O.; Badia, J.D.; Kittikorn, T.; Strömberg, E.; Martínez-Felipe, A.; Ek, M.; Karlsson, S.; Ribes-Greus, A. Hydrothermal Ageing of Polylactide/Sisal Biocomposites. Studies of Water Absorption Behaviour and Physico-Chemical Performance. *Polym. Degrad. Stab.* **2014**, *108*, 212–222. [CrossRef]